BIOINFORMATIC ANALYSIS OF MECHANO-SENSITIVE GENES AND PATHWAYS IN OSTEOCYTE UNDER THE MECHANICAL LOADINGS

Ziyi WANG

2020, October

The Graduate School of Medicine, Dentistry and Pharmaceutical Sciences, Okayama

(Doctor's Course)

OKAYAMA UNIVERSITY, JAPAN

Citations to Previously Published Work

Most of this dissertation from the results reported in the following articles:

1. **Ziyi Wang**, and Hiroshi Kamioka. "The temporospatial pattern of energy metabolism coordinates the interactions between the bones and other organ systems." Journal of Oral Biosciences 60, no. 1 (**2018**): 8-14.
2. **Ziyi Wang**, Yoshihito Ishihara, Takanori Ishikawa, Mitsuhiro Hoshijima, Naoya Odagaki, Ei Ei Hsu Hlaing, and Hiroshi Kamioka. "Screening of key candidate genes and pathways for osteocytes involved in the differential response to different types of mechanical stimulation using a bioinformatics analysis." Journal of bone and mineral metabolism 37, no. 4 (**2019**): 614-626.

Abstract

Background: Review in **Chapter I** discussed the cell-cell communications among bone cells and those between the bone and other organs systems with an emphasis on the role of the energy metabolism. The intercellular network of cell-cell communications among osteocytes is mediated by gap junctions. Gap junctional intercellular communication (GJIC) is thought to play an essential role in the integration and synchronization of bone remodeling. To further understand the mechanism of bone development, it is of great importance to investigate the underlying mechanism of osteocyte differentiation-induced changes of GJIC capacity.

Methods: **Chapter II** emphasized on the mechano-sensitive genes to figure out a possible mechanism for the osteocyte differentiation-induced changes of GJIC capacity. Therefore, a bioinformatics analysis was applied to screen the key genes and pathways that are activated when different types of mechanical loading are applied to osteocytes. We retrieved the public mRNA expression datasets (series number of GSE62128 and GSE42874) from Gene Expression Omnibus database (GEO). High gravity-treated osteocytic MLO-Y4 cell-line samples from GSE62128 (Set1) and fluid flow-treated MLO-Y4 samples from GSE42874 (Set2) were employed. Functional enrichment was performed after the differentially expressed genes (DEGs) were identified. The common DEGs between Set1 and Set2 were considered as key DEGs, and then the minimal nodes from all such key DEGs were used to construct a protein-protein interaction (PPI) network that linked most of the key DEGs. Several open source software programs were employed to process and analyze the original data. The bioinformatic results and the biological meaning were validated by *in vitro* experiments.

Results: Bioinformatic analysis in **Chapter II** demonstrated that high gravity and fluid flow induced opposite expression trends in the key DEGs. The hypoxia-related biological process and signaling pathway were the common functional enrichment terms among the DEGs from Set1, Set2, and the PPI network. The expression of almost all the key DEGs (*Pdk1*, *Ccng2*, *Eno2*, *Egln1*, *Higd1a*, *Slc5a3*, and *Mxi1*) was mechano-sensitive. Eno2, a gene related to adenosine triphosphate generation, was identified as the hub gene in the PPI network, and Eno2 knockdown resulted in expression changes of

some other key DEGs (*Pdk1*, *Mxi1*, and *Higd1a*).

Conclusions: A brief review in **Chapter III** elaborated on the changes of GJIC induced by hypoxia and several hypotheses were proposed for the future studies. Our findings based on the prediction of a bioinformatics analysis indicated that the hypoxia response might have an important role in the differential responses of osteocytes to the different types of mechanical force and the osteocyte differentiation-induced changes of GJIC capacity may be subject to the regulation of hypoxia signal pathway-mediated energy metabolism.

Contents

List of Figures

List of Tables

Abbreviations

α-MEM, Minimum Essential Medium;

ANOVA, analysis of variance;

β2AR, beta 2-adrenergic receptor;

BCS, bovine calf serum;

BMD, bone mineral density;

BP, biological process;

CC, cellular component;

Ccng2, Cyclin G2

cDNA, complementary DNA;

cKO_{col1}, 2.3-kb *Col1a1* promoter knock out mouse model;

Clock, Circadian Locomotor Output Cycles Kaput;

Cx43, connexin43;

DAVID, Database for Annotation Visualization and Integrated Discovery;

DIC, differential contrast microscopy;

DEGs, differentially expressed genes;

Egln1, Egl nine homolog 1, which is also known as prolyl-4-hydroxylase (PHD)

Eno2, enolase 2;

FGF23, fibroblast growth factor 23;

FRAP, fluorescence recovery after photobleaching;

G-CSF, granulocyte colony-stimulating factor;

GDF11, growth differentiation factor 11;

GEO, Gene Expression Omnibus database;

Gja1, gene of connexin43;

GJ, Gap Junction;

GJIC, gap junctional intercellular communication;

glu-OC, undercarboxylated osteocalcin;

GO, gene ontology;

HHO, Havers-Halberg oscillation;

Higd1a, HIG1 domain family member 1A;

HIFBS, heat-inactivated fetal bovine serum;

HSPC, hematopoietic stem/progenitor cell;

KEGG, Kyoto Encyclopedia of Genes and Genomes;

MF, molecular function;

mRNA, messenger RNA;

Mxi1, max-interacting protein 1;

OPG, osteoprotegerin;

PBS, phosphate-buffered saline;

PDIA3, protein disulfide isomerase family A member 3;

Pdk1, pyruvate dehydro- genase kinase 1;

PTH, parathyroid hormone;

PPI, protein–protein interaction;

RANKL, receptor activator of nuclear factor kappa-B ligand;

RT-PCR, quantitative real-time reverse transcription-PCR;

RI, repeat interval;

Runx2, runt-related transcription factor 2;

SDF-1, stromal derived factor-1;

Slc5a3, solute carrier family 5 member 3, which is also known as sodium/myo-inositol transporter 1 (SMIT1)

Chapter I

Cell-Cell Communications in Bone Cells and Between the Bones and Other Organ Systems

I-1 Abstract

Background: Bones adapt to loads by changing their structure. This biomechanical interaction and the formation/maintenance of bones are orchestrated by three major cell types residing in the bones: osteoblasts, osteocytes, and osteoclasts. Recent findings suggest that, in addition to their biomechanical interactions, bones and other organ systems may also communicate biochemically.

Highlight: This brief review will discuss the interaction between the bones and the nervous system, vasculature, muscle, and fat tissues, with an emphasis on the role of the energy metabolism in these interactions.

I-2 Introduction

The bone of terrestrial vertebrates is a part of mechanical system that developed to counteract the force of gravity. Bone is one of the largest tissues in the human body. This important feature of bone implies that bone modeling and remodeling both consume a large amount of energy causing the skeletal system to be difficult to maintain. Bone is also considered to be an endocrine organ that can affect the global metabolism and the balance of energy [1].The primary functions of bone as an organ are the synthesis of biomechanical signals and the interaction with biochemical and neural signals, which maintain the bone mass and bone matrix quality in order to tolerate large physical loads [2].

This chapter is a brief review of the interactions between bone and other organ systems. We will briefly review the current knowledge on the endocrine role of bone and the interactions of bone with the nervous system, vasculature, muscle and fat tissue. We will then discuss the functional significance of these connections, with an emphasis on the role of sclerostin and energy metabolism in these interactions.

I-3 Osteocytes and osteoblasts are endocrine cells

Osteocytes are cells with a dendrite shape that are buried in the mineralized bone matrix. They are connected with each other by a cellular network that is formed by cytoplasmic processes. The gap junctions on those processes provide cell to cell communications mainly formed by connexin43 (Cx43). These processes also form gap junctions with the membrane of osteoblasts and the lining cells that are located at the bone surface. Studies have suggested that osteocytes have an endocrine function [3–5], making the scientific community aware that osteocytes are hormone-releasing cells [6, 7]. The bone cells secrete some hormones that directly fulfill their endocrine function. Fibroblast Growth Factor 23 (FGF23), which regulates the serum phosphate levels is a hormone that is mainly secreted by osteocytes [7]. The ability of osteoblasts to affect the glucose metabolism was revealed by the partial ablation of osteoblasts in transgenic mice, which resulted in profound effects on glucose metabolism and gonadal fat mass, along with increased energy consumption [8].

In addition, bone cells have an important role in mineral homeostasis: they act as a metaphorical "bank of calcium". Additionally, osteocytes may contribute to mineral homeostasis by liberating minerals from the surface of the lacunae in which they reside. This process, called “osteocytic osteolysis” or “perilacunar remodeling” may be mediated by the activation of the parathyroid hormone (PTH) receptor [9]. Osteocytes account for approximately 90-95% of the total cells in bone. The surfaces of osteocytes is 400-fold larger than that of the entire Haversian and Volkmann system [10]. Thus, osteocytic osteolysis might account for more than 90% of the total amount of calcium released via the acidification of the osteocyte lacuna [11].

A recent finding, which showed that the serum calcium concentration was negatively correlated with the lumbar bone mineral density (BMD), is consistent with this hypothesis [12]. Moreover, a study using a genetic approach demonstrated that osteocytes are the main source of receptor activator of nuclear factor kappa-B ligand (RANKL), which plays a role in osteoclast formation in the remodeling of cancellous bone [13]. Thus, osteocytes have an important role in mineral homeostasis,

which can affect the bone mass density.

I-3.1 *The brain-bone-blood triad*

The "brain-bone-blood triad" was introduced by Spiegel *et al*. in 2008 [14]. In this model, the nervous system is the highest proposed regulatory hierarchy and exerts direct and indirect effects on stem cells, the immune system, bone, the bone marrow vasculature, and the supportive stromal microenvironment. Moreover, a study showed that osteocytes, the primary cellular component of mature bone, are regulators of hematopoietic stem/progenitor cell (HSPC) migration [15].

Recent studies have showed that the nervous system plays an important role in various aspects of HSPC biology. The activation of peripheral noradrenergic neurons by granulocyte colony-stimulating factor (G-CSF) could cause the suppression of the function of endosteal bone-lining osteoblasts and a decrease in the level of bone marrow chemokine stromal derived factor-1 (SDF-1), thereby inducing the mobilization of HSPC. Additionally, a beta 2-adrenergic receptor (β2AR) agonist rescues the mobilization defects in mice deficient in dopamine β-hydroxylase and augments G-CSF-induced mobilization [16]. Furthermore, G-CSF also indirectly induces the apoptosis of osteoblasts during HSPC mobilization through the suppression of SDF-1, which is mainly expressed by osteoblasts [17].

Aside from its role in regulating HSPC, the nervous system also richly innervates the skeleton [18]. Recent studies have shown that that inner ear vestibular lesions induced bone loss, especially in the lower limbs, in rats. These studies also showed that β2AR, a protein which is also expressed by osteoblasts, is a key factor in the inner ear vestibular lesions which then caused bone loss [19, 20].

Blood vessels are, in part, the base for bone remodeling, as they provide osteoclast precursors to begin resorption, as well as osteoblast precursors, energy, and waste disposal. Moreover, almost every osteotropic agent has vasculotropic actions [21]. The sustentacular niche for the osteoprogenitor cells is provided by the vasculature throughout the skeletal lifespan [22]. Conversely, the osteoblasts and progenitor cells of the bone marrow create the hematopoietic microenvironment [23] and are regulated

gatekeepers of the egress of hematopoietic cell into the circulation [24].

In summary, the nervous system works as an important regulator of HSPCs, both directly and indirectly, via bone remodeling. Meanwhile, the vasculature provides a crucial basic support for this brain-bone-blood link.

I-3.2 *The interaction between bone with muscle*

Muscles and bones are functionally linked to enable movement of the skeleton and locomotion. It is well-known that muscle forces are necessary for bone development as well as proper bone modeling and remodeling [2]. Moreover, developmental studies have shown that muscle contraction is needed for bone morphogenesis and joint formation during early embryogenesis [25, 26]. A recent study showed a statistical association between the muscle mass and bone architecture in both men and women [27].

In addition to the mechanical coupling between bone and muscle, biochemical communications take place between them. A study using the osteoblast/osteocyte–specific ablation of the Cx43 gene (*Gja1*), which was driven by the 2.3-kb *Col1a1* promoter (cKO_{col1}) in mice, revealed that this *Gja1* deletion in bone cells affects postnatal muscle growth and function, leading to an approximately 30% reduction in muscle mass and an approximately 50% reduction in strength, compared to the normal values [28]. In addition, the *in vivo* rescue experiment of this study showed that the injection of osteocalcin into postnatal cKO_{col1} mice increased the fast muscle cross-section area and restored the muscle strength. This study also showed that the expression of *bglap1* and *bglap2* which encode osteocalcin and circulating undercarboxylated osteocalcin (glu-OC) were significantly reduced in cKO_{col1} mice. Moreover, previous studies demonstrated that Runt-related transcription factor 2 (Runx2, which controls osteoblast differentiation and the expression of *bglap*) is down-regulated in Cx43-deficient osteoblasts. Therefore, they hypothesized that glu-OC influences the muscle growth and function via an endocrine mechanism, and that the deletion of Cx43 might block the regulatory loop between muscle and bone. Myostatin was shown to induce osteoclastogenesis [29]. Growth

differentiation factor 11 (GDF11), which is highly homologous with myostatin, was shown to lead to bone loss in both young and old mice, possibly through stimulating the RANKL-induced formation of osteoclasts [30]. An *in vitro* study in which C2C12 myoblasts were treated with media collected from differentiated osteocytes, demonstrated that osteocytes inhibit myogenesis [31]. This study also identified numerous cytokines that were present in the osteocyte secretome, which might begin to explain how osteocytes inhibit myogenesis. In summary, both mechanical and biochemical communication exist in the interaction between bone and muscle.

I-3.3 *The interaction between bone and fat tissue*

Lipid molecules are a necessary fuel for bone. One-fifth of postprandial lipoproteins are absorbed by bone; this amount is equivalent to the amount absorbed by the liver, but more than the amount absorbed by the heart and muscle. The oxidization of fatty acids in osteoblasts provides from 40–80% of the energy needs of osteoblasts [1].

Leptin, a protein produced by adipocytes, can regulate the food intake by stimulating its receptor in the hypothalamus to suppress satiety signaling. in genetic studies, mice lacking either leptin or its receptor exhibited a high bone mass [32]. Leptin exerts this effect indirectly by activating the sympathetic nerves, which regulate the proliferation and differentiation of osteoblasts by targeting β2AR on these cells [33]. Leptin causes the upregulation of sympathetic tone, which has been shown to indirectly inhibit the secretion of insulin by inhibiting the production of osteocalcin [34]. Osteocalcin, an osteoblast-specific protein, acts as a hormone, causing beta cells in the pancreas to release more insulin, and causing adipocytes to release adiponectin, the hormone that increases sensitivity to insulin [35, 36]. Thus, there is a feedback control loop of energy homeostasis involveing osteoblasts, adipocytes, and the nervous system [7]. Furthermore, recent studies have indicated that osteocytes might also be involved in this control loop through sclerostin, a specific product of osteocytes [37].

Sclerostin is encoded by the *SOST* gene, which is almost exclusively formed by osteocytes and

has anti-anabolic effects on bone formation. Sclerostin is secreted into the circulation and is detectable in serum. Sclerostin inhibits Wnt signaling by binding to the LRP5/LRP6 co-receptors [38]. Wnt signaling is an important determinant of both white and brown adipogenesis [38–40]. Thus, it is possible that sclerostin could also alter adipogenesis. A study showed that sclerostin directly enhances the white adipogenic differentiation of 3T3-LI cells [41]. In a genetic study, mice with high circulating sclerostin levels, achieved through constitutive or inducible loss of the stimulatory subunit of G-proteins in mature osteoblasts and/or osteocytes, showed unchanged serum insulin levels and increased beige adipogenesis [42]. In this study, an osteocytic cell line lacking the stimulatory subunit of G-proteins, and which has a high degree of sclerostin secretion, was engineered, and the conditioned media from these cells significantly increased expression of brown-adipocyte-like uncoupling-protein 1 in primary adipocytes. This finding suggested that sclerostin directly contributes to the regulation of beige adipogenesis. A clinical study also showed that circulating sclerostin levels are associated with higher vertebral marrow fat levels in men [43].

In summary, bone is a part of an endocrine loop linking adipocytes, neurons, and the skeleton to the energy metabolism through leptin, osteocalcin, and sclerostin. Paradoxically, clinical studies have shown that high circulating levels of sclerostin are positively associated with higher bone density [44, 45]. This indicated that the effects of sclerostin are more complex; therefore, the details of this control loop remain unclear.

I-4 Possible key factor underlying the interaction between bone and other organ systems

The development of the various body systems requires highly coordinated signaling systems that coordinate spatial and temporal patterns of cell division, cell differentiation, and morphogenesis. Physiological development requires the creation and coordination of different niches in the body. Bone remodeling involves a dynamic equilibrium, and the maintenance of the steady status of bone presents in a circadian manner [46]. Since the maintenance of the steady status of bone requires stability and various forms of energy support, knowing the role of energy metabolism might be helpful in

understanding the network of connections between bone and other organ systems.

Migration can be induced by various extracellular triggers, including metabolic stress [47]. Sclerostin is an inhibitor of Wnt signaling, the expression level of which can be impacted by mechanical stimuli [48, 49]. Moreover, sclerostin can regulate the production of RANKL [50, 51] and the expression of mineralization-related genes [52, 53]. The following parts will discuss the role of energy metabolism in these potential key mechanisms (migration and sclerostin) of interaction between and the other organ systems.

I-4.1 *Bone cell migration*

Cell migration is a multipurpose process, which allows cells to reach and change their niche in a given environment to execute their function, to form or abandon assemblies with neighboring cells and to move either individually or collectively, and to mechanically and chemically interact with the structural tissue components, thereby alter the interstitial tissue composition and organization [47]. The conception of “niche” that comes from ecology, is very helpful for understanding the body’s “biogeography.” The term “niche” is used to describe a domain that secretes an array of signaling molecules and creates the unique microenvironment required for the maintenance and self-renewal of tissue, organ or a particular cell type, such as mesenchymal stromal cells. A recent study showed that the lung is a major site of platelet biogenesis. In this case, the lung may contain different signaling partners, which create a unique niche for guiding the migration of megakaryocytes to the lungs and promote the release of platelets by megakaryocytes [54].

Energy support might be part of the reason that bone marrow cells travel such a long distance to the lung to fulfill their hematopoietic function. Since the bone takes up one-fifth of the postprandial lipoproteins, this organ system might not have sufficient energy to support the hematopoietic function of all HSPCs. Metabolic stress is one of the extracellular triggers that leads to the induction of migration [47].

Recent studies have demonstrated that the osteoblasts can migrate long distances inside 3D

culture gel (collagen matrices) [55]. In this study, the migration of osteoblasts and their differentiation into early osteocytes inside the dense collagen matrices occurred almost simultaneously with the high expression of matrix metallopeptidase 13, integrin-binding sialoprotein, and Dentin matrix acidic phosphoprotein 1. This study also showed that the migration of osteoblasts is enhanced by the presence of apatite bone mineral. Furthermore, magnesium ions can facilitate the migration of osteoblasts into scaffolds, possibly via the integrin-mediated signaling pathway [56]. Magnesium is a crucial mineral for the energy metabolism of our body system [57].

In summary, cellular migration looks to be a good solution to energy support limitations, and energy support might be a tropic factor that is involved in cellular migration.

I-4.2 *Osteocytes and sclerostin*

Due to the numerous studies about osteocytes, it is well established that osteocytes and their dendritic process network are the main components that orchestrate the function of osteoblasts and osteoclasts following both mechanical and hormonal cues [58]. Due to the influence of the dendritic process network, the bone forms a unique architecture that is termed the lacunar-canalicular system. The spaces within this system are filled with bone fluid and the dendritic processes of osteocytes [37]. The extensive connections between osteocytes and other osteocytes, between osteocytes and osteoblasts, between osteocytes and osteoclasts, and between osteocytes and the vasculature, allow the osteocytes to respond to changes in the bone microenvironment and in the serum [59–61]. Sclerostin, an osteocyte specific protein, can regulate the production of RANKL and the expression of numerous mineralization-related genes (e.g., DMP1, PHEX, MEPE, and FGF23) [37]. The regulation of the sclerostin expression is subject to a complex process of cooperation between different types of factors: physical loading, local signals, and hormonal molecules, all of which are sensed by the osteocyte process network [49].

Additionally, a phase 2 double-blind randomized controlled trial of an anti-sclerostin antibody (romosozumab) supported its potential application in osteoporosis treatment [62]. Thus, sclerostin

might be the major mediator for integrating mechanical, local, and hormonal signals, which are sensed by osteocytes, and in controlling the remodeling apparatus within the individual bone remodeling compartment, a specialized anatomical structure identified at a distinct site of bone remodeling, which is closely associated with the blood vessels [37].

As mentioned above, bone modeling and remodeling consume a great deal of energy; therefore, bone must have the ability to sense the local and global fuel status, and the ability to release certain factors when struggling for energy. Since sclerostin is an inhibitor of Wnt signaling, the Wnt signaling network links the cellular metabolism with cellular biological events [63], which is an important mechanism for modulating the cellular metabolism in osteoblasts. The importance of Wnt signaling during bone formation has been well documented [38, 64]. Taken together, sclerostin might be one of the factors that helps the bone to struggle for energy.

In summary, in the bone organ system, sclerostin is the key regulator of bone modeling and remodeling and its expression level can be impacted by mechanical stimuli and hormonal signals from other organ systems. Serum sclerostin can also impact the global energy metabolism to balance the energy consumption between the bone and other organ systems. However, many details of this pattern remain unknown.

I-5 Summary

As bone is one of the largest organs, its biology is clearly important, and this review demonstrated that it is also complex and interdependent on the biology of many other organ systems.

The concept of a “niche” is very helpful for clarifying the connections between multiple organ systems, as well as strengthening the link between the cell's function and its microenvironment. The cell's migration and differentiation are tropic movements that are induced by a “niche.” It is reasonable to consider the human body system from an ecological viewpoint. Approximately 3.4 billion years passed between the time that the first known single-celled organisms appeared on the earth and the time that the first multicellular animals appeared. At the very beginning, multicellular animals were

essentially comprising a small ecologic system constructed by individual cells, the behavior of which was more like an individual organism. This approach highlights that we should always remember that our body's biological system was not designed; rather, it was formed by evolution and is still evolving. Similarly, energy plays a crucial role in both the ecological niche and the body system. Consequently, the Wnt signaling network, which functions as a bridge linking the energy consumption to the biological function, is extremely important for almost all biological events in the body system.

The limitation of energy support might be the main reason why developmentally differentiated cells without a proliferation function survived natural selection in the body system of multicellular animals. It might also be the reason why proliferative cells cannot perform the function of developmentally differentiated cells. In contrast, most of the developmentally differentiated cells in organisms with relative lower energy consumption, i.e., plants, can easily dedifferentiate and become proliferative again.

Based on the discussion above, cell-cell communications and energy metabolism are very important in bone biology. We therefore hypothesize that the capacity of cell-cell communication may be decreased during the osteocytes' differentiation due to the limited nutrients supply but some of mature osteocytes may still keep high capacity of cell-cell communication in order to "monitor" the mechanical stimuli. In addition, the energy related signal pathways or genes may play a crucial role in the differential responses of osteocytes to the different types of mechanical force.

Our previous work [65] had quantified the difference in the GJIC capacity between young and developmentally mature osteocytes. First, an embryonic chick calvaria growth model (ECCGM) was established to show the growth of the calvaria in embryos at 13 to 21 days of age. The relationship between the longest medial-lateral length of the calvaria (frontal bone) and the embryonic age fit a logarithmic growth model: length = $5.144 \times \ln(\text{day}) - 11.340$. The morphometric data during osteocyte differentiation showed that the cellular body becomes more spindle-shaped and that the cell body volume decreased by approximately 22%with an increase in the length of the processes between the

cells. However, there were no significant differences in the cellular body surface area or in the distance between the mass centres of the cells. Afterward, the difference in the GJIC capacity of young osteocytes was compared with that of developmentally mature osteocytes using the fluorescence recovery after photobleaching (FRAP) technique. Results from FRAP showed that the dye-displacement rate in young osteocytes was significantly higher than that in developmentally mature osteocytes. Specifically, dye displacement occurred in only 26.88% of the developmentally mature osteocytes but in 64.38% of the young osteocytes. Finally, the dye (Calcein) diffusion from the FRAP data was quantified by adopting a mathematic model of simple diffusion, which was also employed to identify simple diffusion GJIC pattern cells (fitted model) and accelerated diffusion GJIC pattern cells (non-fitted model). In all recovered osteocytes, 36% of the developmentally mature osteocytes were of non-fitted model cells, while 53.19% of the young osteocytes were of the non-fitted model, which indicates the active transduction of dye molecules. However, no statistically significant differences were observed between the young and developmentally mature osteocytes with regard to the diffusion coefficient, permeability coefficient, or permeance of the osteocyte processes, which were 3.93 ± 3.77 (×10-8cm2/s), 5.12 ± 4.56 (×10-5cm2/s) and 2.99 ± 2.47 (×10-13cm2/s) (mean ± SD), respectively. Our findings in this previous work [65] suggested that GJIC in mature osteocytes had the same permeability as the young osteocytes but there were fewer mature osteocytes with a functioning GJIC (dye displacement occurred) than young osteocytes.

In the **Chapter II** study, to find a possible underlying mechanism of osteocyte differentiation-induced changes of GJIC capacity, we screened out and primarily validated some candidate genes that showed extremely mechano-sensitive expression levels when different types of mechanical stimuli are applied using a bioinformatics analysis. In **Chapter III**, A brief review discussed the hypoxia induced changes of GJIC that have been reported in other cell type but not osteocyte. Several hypotheses were proposed in **Chapter III** for the future studies.

Chapter II

Screening of Key Candidate Genes and Pathways for Osteocytes Involved in the Differential Response to Different Types of Mechanical Stimulation Using a Bioinformatics Analysis

II-1 Abstract

This study aimed to predict the key genes and pathways that are activated when different types of mechanical loading are applied to osteocytes. mRNA expression datasets (series number of GSE62128 and GSE42874) were obtained from Gene Expression Omnibus database (GEO). High gravity-treated osteocytic MLO-Y4 cell-line samples from GSE62128 (Set1), and fluid flow-treated MLO-Y4 samples from GSE42874 (Set2) were employed. After identifying the differentially expressed genes (DEGs), functional enrichment was performed. The common DEGs between Set1 and Set2 were considered as key DEGs, then a protein–protein interaction (PPI) network was constructed using the minimal nodes from all of the DEGs in Set1 and Set2, which linked most of the key DEGs. Several open source software programs were employed to process and analyze the original data. The bioinformatic results and the biological meaning were validated by in vitro experiments. High gravity and fluid flow induced opposite expression trends in the key DEGs. The hypoxia-related biological process and signaling pathway were the common functional enrichment terms among the DEGs from Set1, Set2 and the PPI network. The expression of almost all the key DEGs (*Pdk1*, *Ccng2*, *Eno2*, *Egln1*, *Higd1a*, *Slc5a3*, and *Mxi1*) were mechano-sensitive. Eno2 was identified as the hub gene in the PPI network. Eno2 knockdown results in expression changes of some other key DEGs (*Pdk1*, *Mxi1*, and Higd1a). Our findings indicated that the hypoxia response might have an important role in the differential responses of osteocytes to the different types of mechanical force.

II-2 Introduction

FRAP findings in our previous work [65] showed that GJIC in mature osteocytes had the same permeability as the young osteocytes but fewer mature osteocytes with the functioning GJIC (dye

displacement occurred) than young osteocytes. To investigate the possible mechanism underlying this phenomenon that we observed before [65], bioinformatic analysis was applied to screening vital candidate genes and pathways for sensing mechanical stimuli in osteocytes.

More than a century ago we already knew that the trabecular structure of bone was closely related to its mechanical loading (Wolff's Law). It seems that bone cells can sense the different force-direction, force-strength and force-type and respond to them differentially. *In vivo*, osteocytes are usually influenced by several forces, including body forces (e.g., gravity) and surface forces (fluid shear stress, tensile, and compressive stress), which are applied in different directions or with different strength. A body force acts throughout the volume of a body and will cause an object to accelerate, which contrasts with surface force, which is exerted on the surface of an object. The elucidation of the mechanisms underlying these phenomena may be important for understanding the regulation of bone remodeling by a locally acting mechanical force. Bone remodeling is a dynamic process that involves a delicate equilibrium between the function of osteoblasts and osteoclasts. However, research has shown that other cells are involved in this process, most notably osteocytes, which are now considered to be essential players in the process through which the bone senses different types of mechanical force (e.g., pressure, tension, fluid flow and shear stress, etc.) [49]. The clarification of the mechanism underlying the differential responses of bone to various mechanical stimuli is very important for developing novel therapeutic approaches to bone diseases.

Osteocytes, cells with a stellate shape and which are embedded into the mineralized bone tissue, are the most abundant cells in the bone. They are connected with each other via a cellular network formed by their cytoplasmic processes. This osteocyte network has long been thought to play a central role in regulating bone modeling and remodeling by detecting mechanical stimuli to the skeleton through interstitial fluid flow [66, 67] or deformation of the cell body [59]. It is also known that osteocytes are able to orchestrate the function of osteoblasts and osteoclasts [37, 68]. In particular, a previous study reported that osteocytes but not bone surface cells (osteoblasts, osteoclasts, *etc.*),

responded to dynamic mechanical loading in the long bones with multiple Ca^{2+} spikes [69].

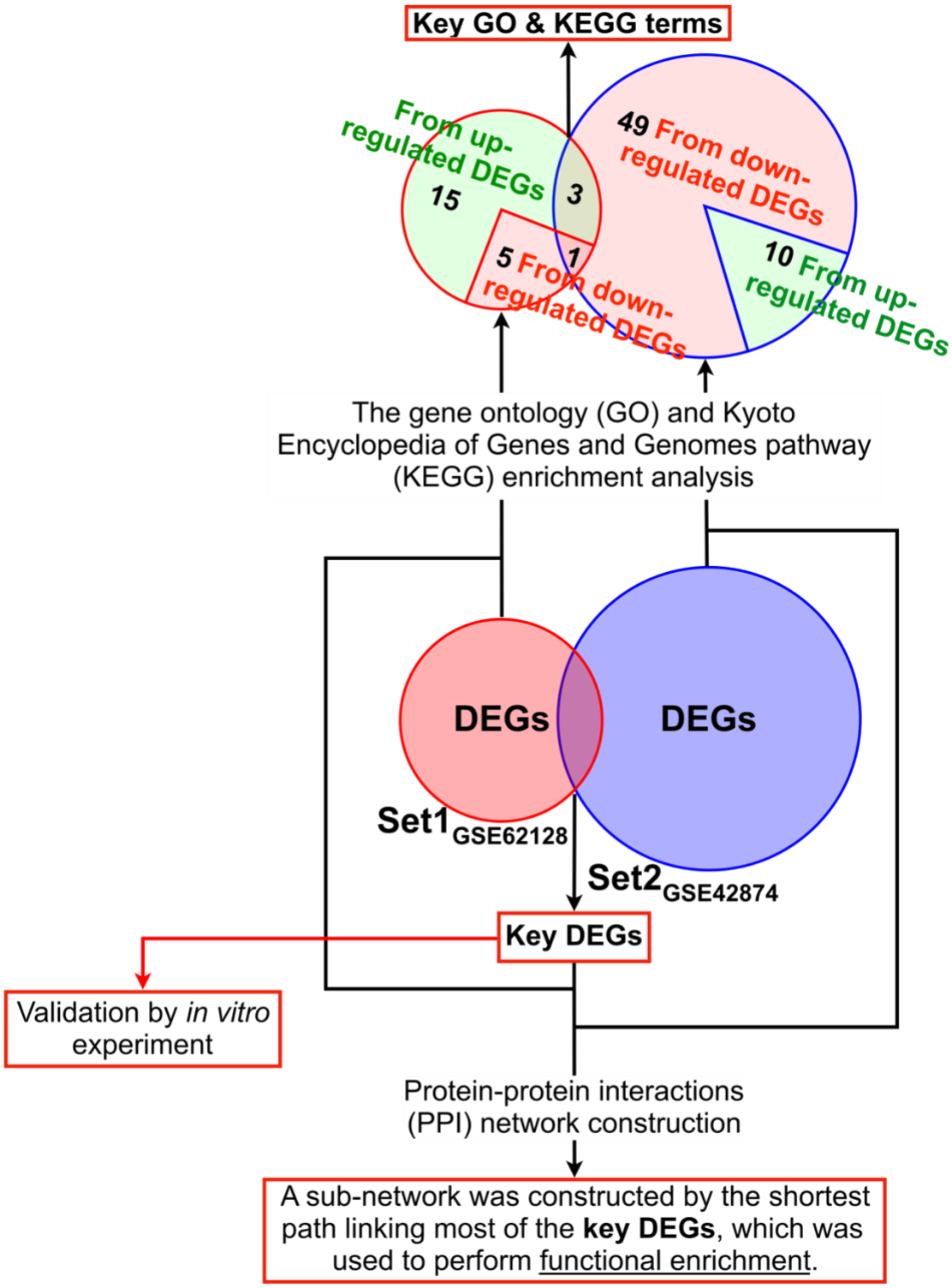

Fig. II-1. The work flow of the present study.
DEGs: differentially expressed genes.

We hypothesized that osteocytes may be an essential part of the process through which bone differentially responds to various types of mechanical stimuli. To test this hypothesis, we screened the

differentially expressed genes (DEGs) of the datasets from the Gene Expression Omnibus (GEO) database to investigate the mechanism underlying this process (**Fig.** II-1). GSE62128 and GSE42874, which exposed MLO-Y4 to different types of mechanical stimuli, were used to screen out the key DEGs for further examination in a functional and pathway enrichment analysis. Finally, the expression levels of key DEGs were validated by several *in vitro* experiments.

II-3 Materials and Methods

II-3.1 Acquisition of microarray data

The raw data with CEL files of three 2-fold gravity of Earth-treated (performed using a large-gradient, high-magnetic-field) (GSM1520101, GSM1520102, GSM1520103) and 3 gravity of Earth-treated (GSM1520104, GSM1520105, GSM1520106) murine long bone osteocyte Y4 (MLO-Y4) samples of GSE62128 (Set 1), and the raw data with CEL files of three 2-hour fluid flow-treated (GSM1052656, GSM1052657, GSM1052658) and 2-hour sham-treated (GSM1052653, GSM1052654, GSM1052655) MLO-Y4 samples of GSE42874 (Set 2) were obtained from the Gene Expression Omnibus (GEO) (http://www.ncbi.nlm.nih.gov/geo/).

II-3.2 Identification of differently expressed genes (DEGs)

The screening threshold was a false discovery rate (FDR) corrected P-value of <0.1 (also known as the q-value) and a $|\log_{2\text{Fold Change}}|$ value of >0.59 (1.5-fold increase or 34% decrease). The raw data with the CEL files of Set1 and Set2 were background corrected, normalized, annotated and log2 transformed using the xps package (https://bioconductor.org/packages/release/bioc/html/xps.html) in *R*. Empirical Bayes statistical tests using moderated genewise variance were performed using the limma package [70] for *R*. If multiple probes correspond to one gene, only the most significant (smaller q-value) result is kept. The DEGs were then identified according to the criteria of a $|\log_{2\text{Fold Change}}|$ value of >0.59 and a q-value of <0.1. The common DEGs between Set1 and Set2 were considered as the key DEGs.

Scripts written in the *R* programming language to allow all of the above-described data processing

procedures and detailed instructions to allow for the reproduction of our results are available from GitHub (https://github.com/wong-ziyi/Microarray_Analysis).

II-3.3 *The biological function and pathway enrichment analysis of DEGs from Set1 and Set2*

To investigate the functional difference when different mechanical forces are applied, biological function and pathway enrichment analyses were performed for Set1 and Set2. Gene Ontology (GO; http://www.geneontology.org) [71, 72] is a tool used for the unification of biological functions based on gene annotation information, which primarily consists of biological process (BP), molecular function (MF), and cellular component (CC) analyses. The Kyoto Encyclopedia of Genes and Genomes (KEGG; available at http://www.genome.ad.jp/kegg/) [73] is a pathway-associated database that connects known information on molecular interaction networks. To understand the biological significance of the identified DEGs, the upregulated DEGs of Set1, the downregulated DEGs of Set1, the upregulated DEGs of Set2 and the downregulated DEGs of Set2 were separately input into the Database for Annotation Visualization and Integrated Discovery (DAVID; http://david.abcc.ncifcrf.gov/) [74] for the GO term and KEGG pathway analyses. An EASE Score (a modified Fisher Exact P-Value) of <0.01 and a gene count of >2 were considered to indicate a statistically significant difference. The common functional terms or the KEGG pathways between Set1 and Set2 were considered to be the key biological process and pathways.

II-3.4 *PPI network construction*

The Search Tool for the Retrieval of Interacting Genes database (STRING) [75] database (https://string-db.org/) provides comprehensive information on the functional interactions between DEGs by calculating their combined score. Using a minimum required interaction score of 0.15 (low confidence), PPI networks were constructed based on the PPI pairs from the key candidate DEGs and the remaining 308 DEGs (**Fig.** II-2) from Set1 and Set2 using the Cytoscape software program (version 3.6.0) (available at http://cytoscapeweb.cytoscape.org/) [76]. Then Pesca 3.0 (a Cytoscape software application) was applied to screen out a subnetwork that was constructed using the minimal nodes

linking all key candidate DEGs. Finally, we retrieved the KEGG enrichment of this subnetwork in the Cytoscape software program using the STRING enrichment application programming interface (API). We analyzed the topological properties of this subnetwork using the tYNA web interface (http://tyna.gersteinlab.org/) [77]. In the nodes with a degree that was greater than or equal to the sum of the mean and the standard deviation (SD), the one that has highest mean interaction score was selected as a key hub gene. STRING also allows users to retrieve the functional enrichment (GO terms and KEGG pathway). The significant functional enrichment terms were identified according the criterion of FDR <0.05.

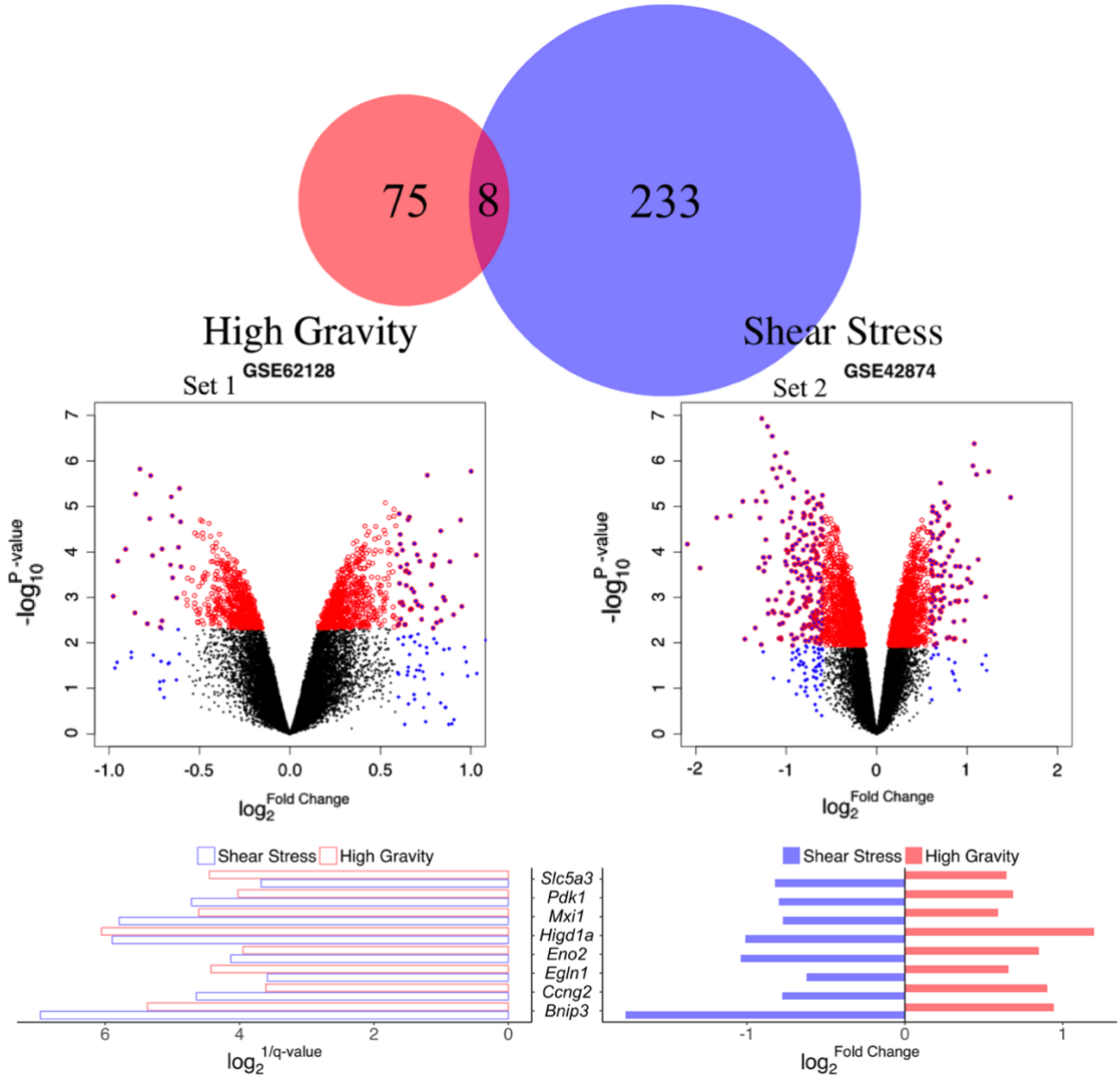

Fig. II-2. Overview of the DEGs from Set1 and Set2.
The significance and the expression levels of the common DEGs in these two datasets are shown in the bottom panel. the expression levels of the common DEGs showed totally opposite trends in Set1 and Set2.

II-3.5 *Fluid flow exposed osteocytic MLO-Y4 cells*

The design we employed was described in our previous study [78]. Briefly, the cells were subjected to fluid flow in a parallel plate flow chamber (Waken Denshi Co.) connected to a flow loop apparatus that was modified from the apparatus described by Frangos et al. [79] to accept quartz glass microscope slides. Osteocytic MLO-Y4 cells (a mouse osteocytic cell line) were cultured on collagen I-coated glass slides in α-modified Minimum Essential Medium (α-MEM; Invitrogen) with 5.0% heat-inactivated fetal bovine serum (HIFBS; HyClone) and 5.0% bovine calf serum (BCS; HyClone) and antibiotics for 2 days and then exposed for 2 h to sinusoidally oscillating fluid flow in parallel plate flow chambers, inducing 2.5 dyn/cm$_2$ or 50 dyn/cm$_2$ shear stress. Paired sham controls were maintained on the same glass slides.

II-3.6 *Compressed osteocytic MLO-Y4 cells*

As described in our previous study [80], osteocytic MLO-Y4 cells were cultured on collagen I-coated glass plates that were maintained in 6-well plates in α-MEM with 5.0% HIFBS and 5.0% BCS and antibiotics for 2 days and then exposed (by direct contact) for 2 h to weights (0.051 g/cm$_2$), inducing 50 dyn/cm$_2$ of continuous compression force.

II-3.7 *Eno2 gene silencing by the siRNA*

Eno2 siRNA (Mission® siRNA select SASI_Mm01_00106092) and negative control siRNA (Mission® siRNA select Mission_Negative control SIC_001) were purchased from Merck (Germany). siRNA was delivered into the cells by electroporation using an Amaxa™ Human Chondrocyte Nucleofector™ kit and an Amaxa Nucleofector® II (Lonza Cologne GmbH, Cologne, Germany) according to the manufacturer's instructions. In brief, 4.0×10$_5$ MLO-Y4 cells were transfected with 100 nM siRNAs in the solution for electroporation (Nucleofector solution and supplement: 100 μL) using electroporation program U-024. Next, cells in α-MEM supplemented with 5% HIFBS and 5% BCS were seeded at a density of 4.0×10$_5$ cells/well into a six-well plate for RNA extraction and incubated at 37°C under 5% CO_2 in air. After 48 h, the cells were collected for subsequent analyses.

II-3.8 *Quantitative real-time reverse transcription-PCR (RT-PCR)*

ISOGEN (Nippon Gene) and a ReverTra Ace qPCR RT Kit (Toyobo) were used to extract total RNA and to synthesize complementary DNA (cDNA), respectively. The resulting cDNA products were used as a template to quantify the relative content of messenger RNA (mRNA) by a quantitative real-time reverse transcription-PCR (RT-PCR). The relative levels of the PCR products were determined using a LightCycler System (Roche Diagnostics). SYBR green chemistry was used to determine the mRNA levels of the key DEGs and GAPDH, a housekeeping gene, in MLO-Y4 cells. The primers showed in **Table** II-1 were used.

Table II-1. The sequences of primers.

Template strand	Sequence (5'->3')	Target Gene	Target Transcript ID
Plus	CATACAGCCGCAGGTTGG	Pdk1	NM_172665.5 // XM_011239444.1
Minus	GAAGTCCAGGAACTGCTTCA		
Plus	CGAGTTGTCTTCTCCAAAGC	Ccng2	NM_007635.4
Minus	CGCGAAACAATCCATACCAG		
Plus	AGCTAAGGTTACCCACGAAC	Bnip3	NM_009760.4
Minus	CAACAAAACTGACCACCCAA		
Plus	CGTCACGTTGATAACCCAAA	Egln1	NM_053207.2
Minus	CGTATGCTGGCTGTACTTCA		
Plus	TCATACGATGAAGGTCAGGG	Higd1a	NM_019814.5 // NM_001357837.1 // 001357838.1 // 001357839.1 // NM_001357840.1 // NM_001357841.1
Minus	GCTCTTCAGCTTGTACAACC		
Plus	TCCAGCACCTGAGTAAATGC	Slc5a3	NM_017391.3
Minus	TTGGTTTGCTGTCTTGATGG		
Plus	AGCTTGGTCCAAGTTCACAG	Eno2	NM_013509.3 // NM_001302642.1
Minus	CTTGAGCAGCAAACAGTTGC		
Plus	TCGTGCTCTACAAAAGGAGA	Mxi1	NM_001008543.3 // NM_001008542.3 // NM_010847.4 // XM_006526741.2
Minus	CACCGAGGCACACAGAG		

II-3.9 *Statistical analysis*

A one-way analysis of variance (ANOVA) with the Holm-Sidak post hoc test was used to identify the statistical significance of the results from cells exposed to different force-direction or force-strength. An unpaired *t*-test was used to compare the differentially expressed genes under hub gene knock-down. Pearson correlation test was applied to investigate the correlation between the hub gene and other

target genes.

II-4 Results

II-4.1 The differential expression analysis

Gene expression profile Set1 (from GSE62128) and Set2 (from GSE42874) identified 83 and 241 DEGs, respectively (**Fig.** II-2, see the entire list in the **Appendix Table 1** and **2**). The common DEGs (*Slc5a3, Pdk1, Mxi1, Higd1a, Eno2, Egln1* and *Bnip3*) across Set 1 and Set 2 were taken as key DEGs. Notably, all key DEGs showed opposite expression trends between Set1 and Set2 (**Fig.** II-2, right side on the bottom panel).

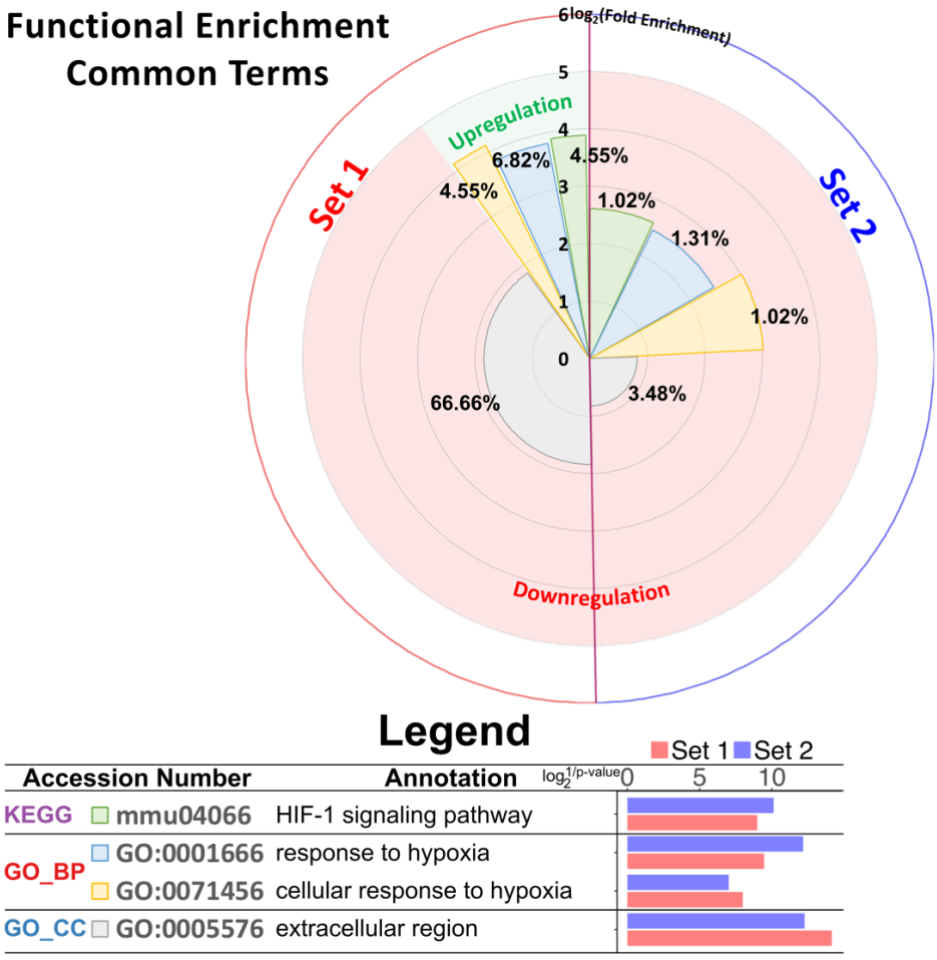

Fig. II-3. Common functional enrichment terms in Set1 and Set2.
In this rose plot, the height of each slice represented the log2 (fold enrichment) value. The radian of each slice represented the percentage of the DEGs covering the corresponding term in relation to all queried DEGs; the exact percentage is shown on the label of each slice. A red background indicates that the terms came from downregulated DEGs. A green background indicates that the terms came from upregulated DEGs. The entire list of the enrichment terms from Set1 and Set2 is shown in in **Appendix Fig. 1** and **2**.

II-4.2 The functional and KEGG pathway enrichment analysis of DEGs from Set1 and Set2

The upregulated DEGs from Set1 and the downregulated DEGs from Set2 that were enriched in the same BP and KEGG terms were mainly associated with the response to hypoxia (**Fig.** II-3). The entire functional enrichment terms are listed in **Appendix Fig. 1** and **2** for Set1 and Set2 respectively.

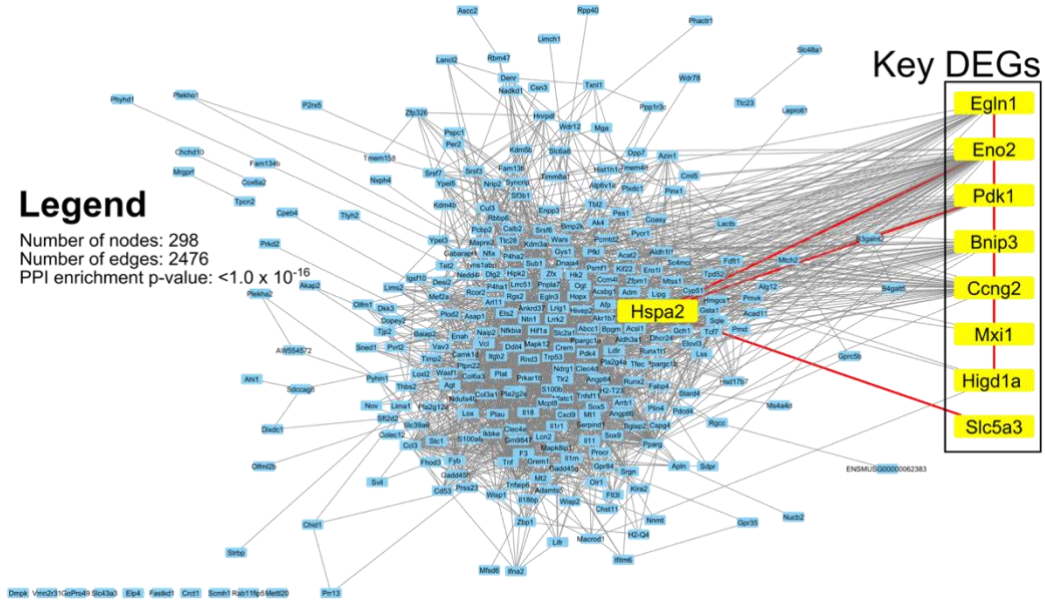

Fig. II-4. Original protein-protein interaction (PPI) network.
Protein-protein interaction (PPI) network was constructed from all the 316 DEGs from both Set1 and Set2. This network contained 298 nodes and 2476 edges with enrichment p-value of $<1.0\times10^{-16}$.

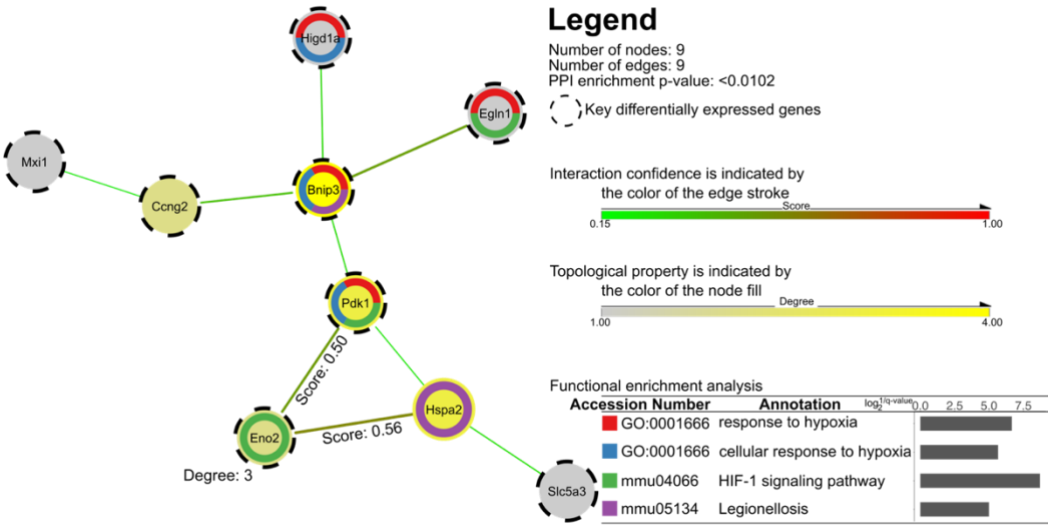

Fig. II-5. The final PPI network.
The final PPI network was a sub-network linking all of the key candidate DEGs from the origin network in **Fig.** II-4. This subnetwork contains 9 nodes and 9 edges with enrichment p-value of <0.0102. In this subnetwork, the interaction confidence is indicated by the color of edge stroke and the topological property is indicated by the color of the node fill. Eno2 with the degree of 3 and mean interaction confidence of 0.53 was identified as the hub gene. The functional enrichment terms were mainly related to the hypoxic response.

II-4.3 The PPI network and the corresponding KEGG pathway enrichment analysis

The PPI network generated from the DEGs of both Set1 and Set2 included a total of 298 nodes and 2476 edges (**Fig.** II-4). Then a subnetwork was constructed by the minimal nodes linking the most key candidate DEGs (Egln1, Eno2, Pdk1, Bnip3, Ccng2, Mxi1, Higd1a and Slc5a3). This subnetwork contained a total of 9 nodes and 9 edges; the enriched BP and KEGG terms were mainly associated with the response to hypoxia (**Fig.** II-5). Eno2 with a degree of 3 and a mean interaction score of 0.53 was selected as the hub gene (**Fig.** II-5).

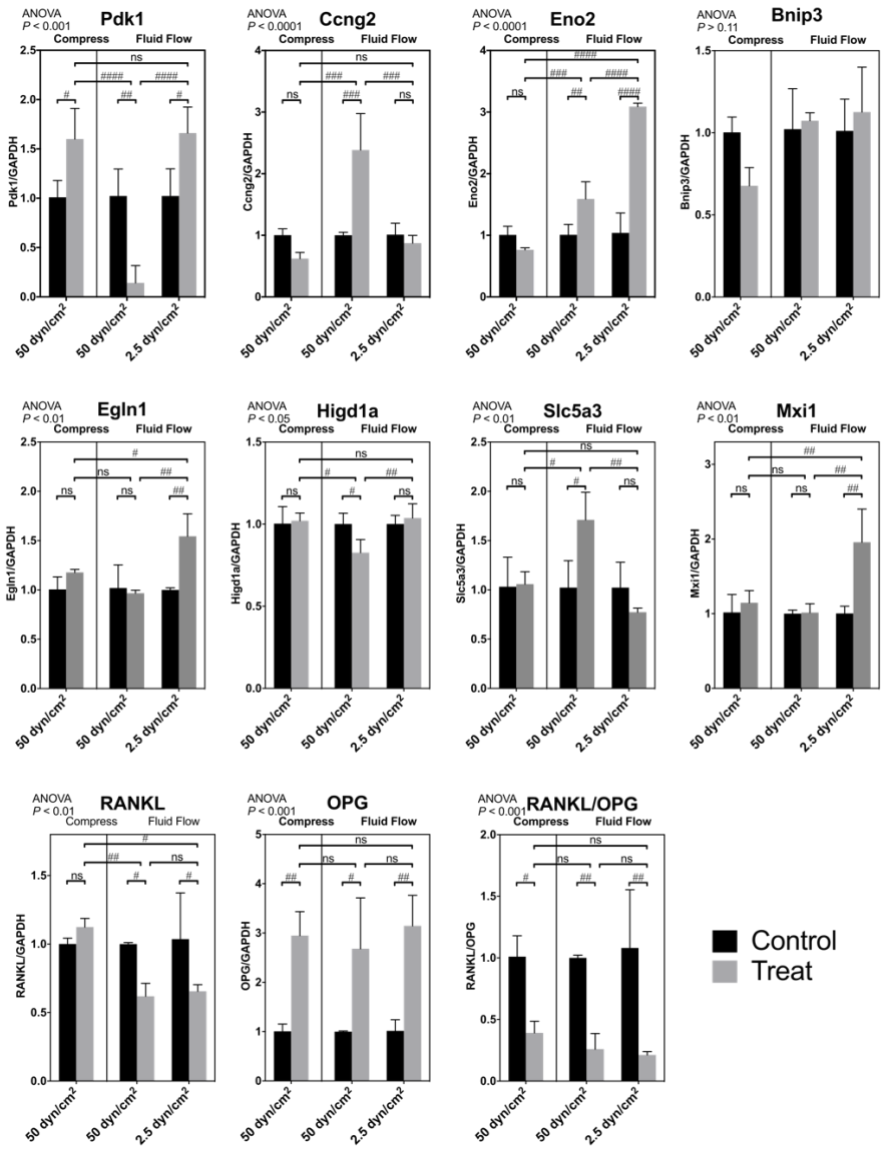

Fig. II-6. Gene expression under mechanical stimuli in MLO-Y4 cells.
The expression of key candidate DEGs and RANKL & OPG under different force-direction with 50 dyn/cm2 or under different force-strength with shear stress from 2.5 dyn/cm2 to 50 dyn/cm2. (#, Holm–Sidak post hoc test in a one-way ANOVA; #, P <.05; ##, P <.01; ### P <.001; #### P <.0001. All values represent the mean ± standard deviation)

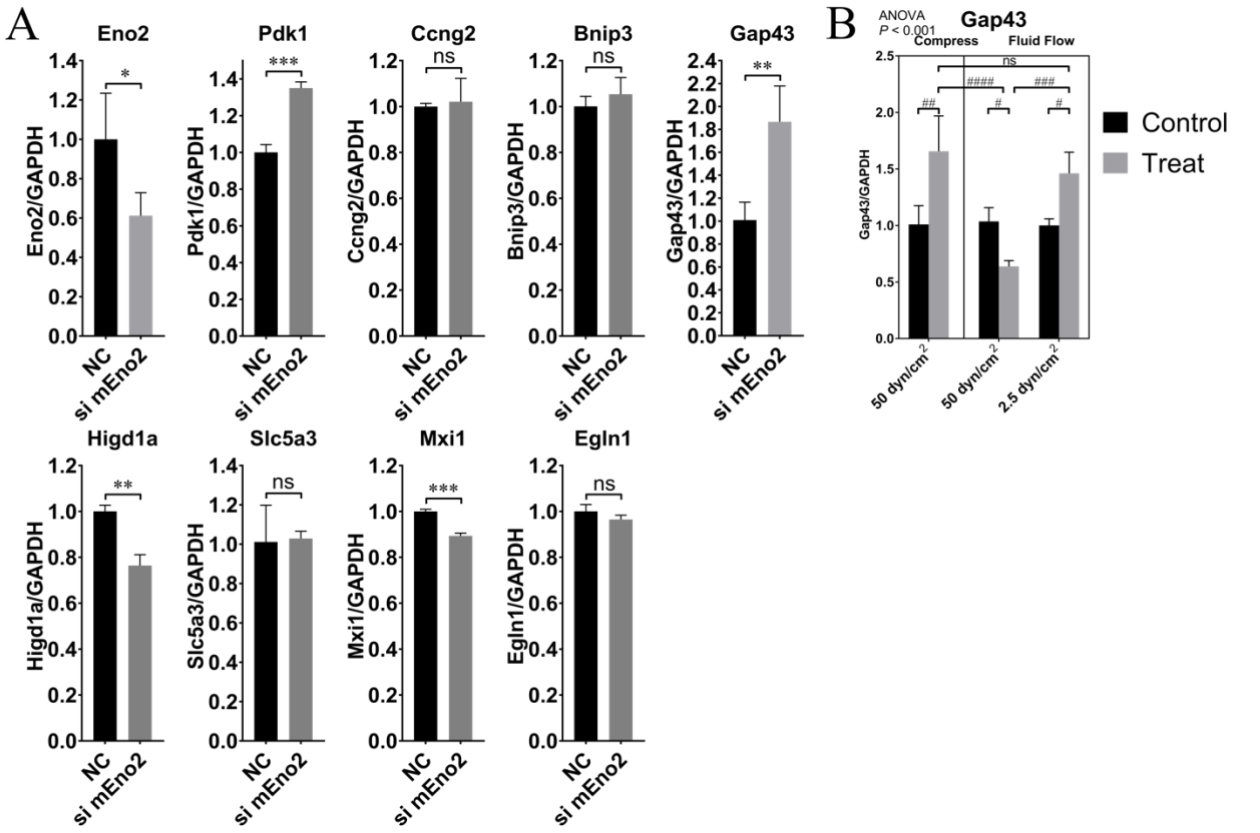

Fig. II-7. Results of Eno2 knockdown.
(**A**) The siRNA of *Eno2* significantly reduced the expression of Eno2, Higd1a and Mxi1 while significantly increased the expression of Pdk1 and Gap43. (*, unpaired *t*-test; *, *P* <.05; **, *P*<.01; NC, negative control; si mEno2, Eno2 siRNA). (**B**) The expression of Gap43 in normal cells under different force-direction or force-strength conditions (#, Holm–Sidak post hoc test in a one-way ANOVA; #, *P* <.05; ##, *P* <.01; ### *P* <.001; #### *P* <.0001). (all values represent the mean ± standard deviation)

II-4.4 *Verification of the mechano-sensitive expression and biological meaning of the key DEGs*

The RT-PCR revealed that among the key DEGs, the expression of *Slc5a3*, *Pdk*, *Mxi1*, *Higd1a*, *Eno2*, and *Egln1* was mechano-sensitive. In addition, all of these genes showed response to a change of the force-strength of shear stress or a change of the force-direction. These genes showed more mechano-sensitivity than the *RANKL*/*OPG* ratio (Error! Reference source not found.). *Eno2* knockdown resulted in a significant increase in the expression of *Pdk1*, *Higd1a*, *Mxi1* and *Gap43* (**Fig.** II-7**A**). A heatmap that was converted from the results showed in Error! Reference source not found. and **7B** with a Pearson correlation test together to investigate the correlation of the Eno2 and expression of other genes (Pdk1, Higd1a, Mxi1, and Gap43) under different force-direction or force-strength conditions (**Fig.** II-8). **Fig.** II-8 showed a significant correlation between the expression of *Eno2* and *Mxi1*. No significant correlation between the expression of *Eno2* and *Gap43*/*Higd1a* was observed in cells

subjected to <2.5 dyn/cm2 in mechanical force, while a strong and significant correlation (**Fig.** II-8) was observed under extreme high mechanical force (50 dyn/cm2). However, we did not observe any significant correlation between the expression of *Eno2* and *Pdk1*.

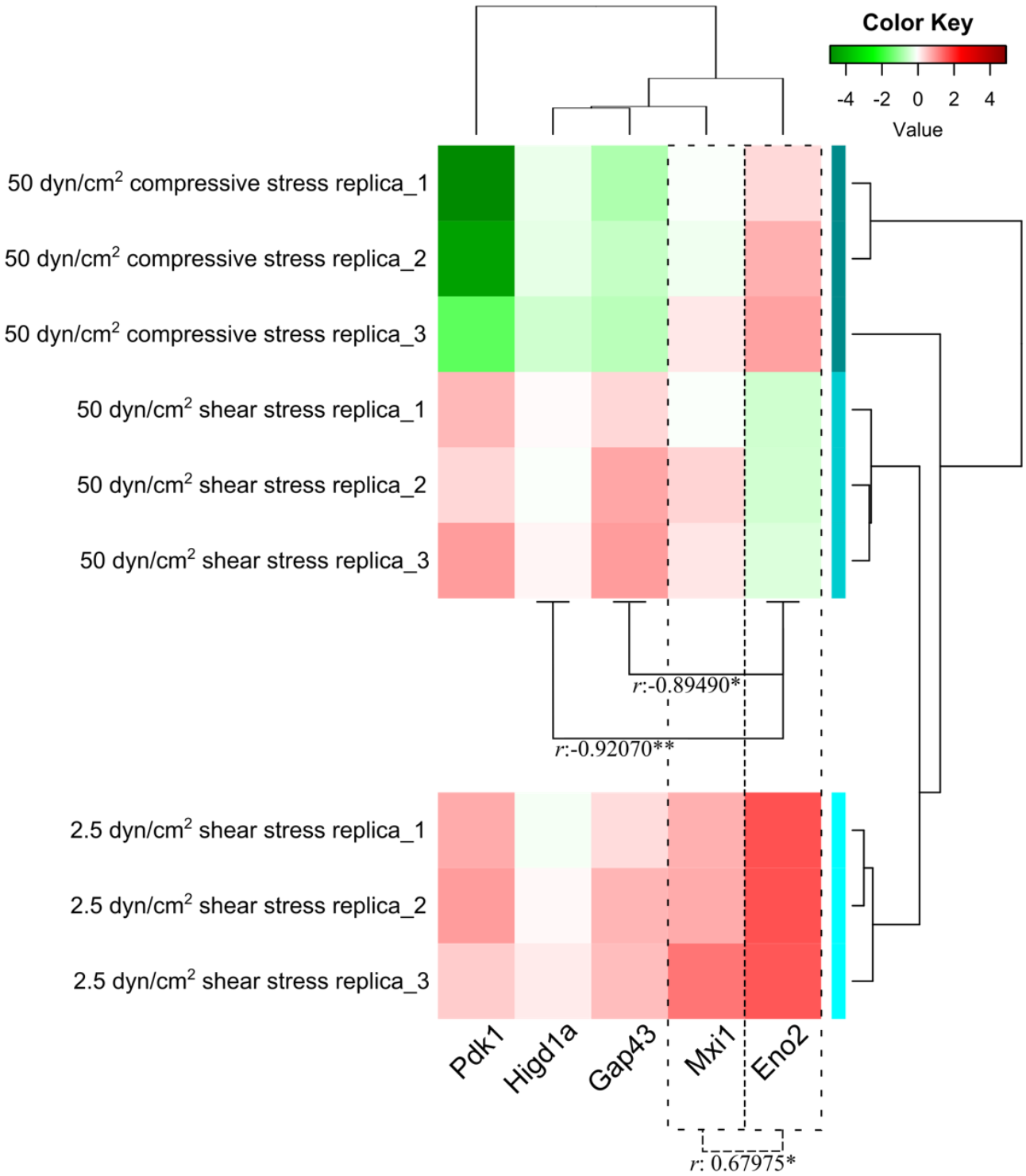

Fig. II-8. A heatmap to show the co-expression
We converted the results from both **Fig.** II-6 and **7B** to create a heatmap with Pearson correlation test to investigate the correlation of the Eno2 and expression of other genes (Pdk1, Higd1a, Mxi1, and Gap43) under different force-direction or force-strength conditions. (*r*, Pearson correlation coefficient; *, *P* <.05; **, *P*<.01)

II-5 Discussion

The present study aimed to screen out the key candidate genes and pathways in osteocytes during the application of different types of mechanical stimuli (high gravity and shear force). We screened out eight common DEGs (*Slc5a3, Pdk1, Mxi1, Higd1a, Eno2, Egln1* and *Bnip3*) across Set1 and Set2, which were selected as candidate key DEGs for further investigation. The functional enrichment indicated that the biological processes related to the response to hypoxia and the HIF-1 signaling pathway had important roles in the mechano-transduction of osteocytes.

II-5.1 *The mechano-sensitive expression of the key candidate DEGs*

High gravity and shear force had an opposite influence on all of the key DEGs (**Fig.** II-2, downregulated by high gravity and upregulated by shear force), which suggested that the osteocytes could sense and recognize different types of mechanical stimuli. To validate this finding from the microarray data, we investigated the expression of these key DEGs in MLO-Y4 osteocytes during shear stress under different conditions of force-strength or force-direction.

The RT-PCR revealed that, with the exception of *Bnip3*, the expression of the rest of the key DEGs in response to mechanical stress with a different force-strength or force-direction was mechano-sensitive (**Fig.** II-6). Notably, the expression of *Pdk1*, *Ccng2*, *Eno2* and *Higd1a* showed opposite trends in response to a different force-direction (**Fig.** II-6, compression vs shear stress under 50 dyn/cm$_2$) which is similar to the results revealed by microarray data, in which the expression showed opposite trends in response to shear stress and high gravity (**Fig.** II-2). Eno2, the hub gene that suggested by the subnetwork (**Fig.** II-5), also showed more sensitivity to the mechanical force than other key DEGs (**Fig.** II-6). On the other hand, *Eno2* knockdown results in significant changes of other three key DEGs (*Pdk1*, *Higd1a*, and *Mxi1*; see in **Fig.** II-7**A**), and co-expression pattern between *Eno2* and *Mxi1*/*Higd1a* (**Fig.** II-8). These results suggested that Eno2 might play a center role in the mechano-transduction of osteocytes to link the key DEGs.

Mechanical loading has been reported to create tears in the cell membrane called plasma

membrane disruptions (PMDs) [81]. In that study, shear stress of 30 dyn/cm2 created PMDs in more than 30% of osteocytes, while shear stress of 10 dynes/cm2 created PMDs in less than 5% of osteocytes *in vitro*. Thus, in the present study, shear stress of 2.5 dynes/cm2 and 50 dynes/cm2 were defined as extremely low and extremely high mechanical force respectively. Even under extremely low shear stress (2.5 dynes/cm2), the expression levels of *Pdk1*, *Eno2*, *Egln1*, *Mxi1*, *RANKL*, *OPG*, and *RANKL*/*OPG* ratio showed significant changes. Moreover, the force-strength change of shear stress from 2.5 dynes/cm2 to 50 dynes/cm2 also induced significant changes in the expression of *Pdk1*, *Ccng2*, *Eno2*, *Egln1*, *Higd1a*, *Slc5a3*, and *Mxi1*, but not *RANKL*, *OPG*, and the *RANKL*/*OPG* ratio. Similarly, the force-direction change from shear force to compression induced significant changes in the expression of *Pdk1*, *Ccng2*, *Eno2*, *Higd1a*, *Slc5a3*, and *RANKL* but not *OPG* or the *RANKL*/*OPG* ratio (**Fig.** II-6). These results indicated that the expression of *Slc5a3*, *Pdk1*, *Mxi1*, *Higd1a*, *Eno2*, and *Egln1* is more mechano-sensitive than that of *RANKL* and *OPG*.

Intriguingly, most of these mechano-sensitive genes (Egln1, Pdk1, Mxi1, and Slc5a3) clearly showed roles in bone development, modeling and remodeling—especially Egln1 and Pdk1, mechano-sensitive genes that are related to the hypoxic response (**Fig.** II-5 bottom panel).

II-5.2 *A potential key pathway through which various types of mechanical stimulation are recognized in osteocytes*

Hypoxia-inducible transcription factor (HIF), is one of the key factors in the regulation of the function of osteoclasts and osteoblasts. The HIF heterodimer is composed of an inducible alpha subunit (HIF-1α, HIF-2α) and a constitutively expressed beta subunit (HIF-β/ARNT). Egl nine homolog 1 (Egln1), which is also known as prolyl-4-hydroxylase (PHD) domain-containing protein 1, is one of the PHD enzymes (PHD1-3). PHD enzymes, as a type of proteasome, degrade the HIF-α by hydroxylation, which results in the post-translational regulation of HIF. Previous studies have shown that the combined osteoblast-specific deletion of Egln2 with either Egln1 and/or Egln3 increased trabecular bone formation [82]. Similarly, the stabilization of HIF by inhibitors of PHD enzyme improved

fracture healing, increased the bone mineral density and bone strength in murine models of bone fracture [83–86], distraction osteogenesis [87], and osteoporosis [88, 89].

On the other hand, the induction of pyruvate dehydrogenase kinase 1, the protein encoded by Pdk1, is directly regulated by HIF-1α, which in turn inhibits the activity of pyruvate dehydrogenase and thereby blocks the mitochondrial tricarboxylic acid cycle (TAC). As a consequence, the activity of HIF-1α could reduce the collagen hydroxylation, which was reported by a previous study [90]. Notably, HIF1 could directly regulate the expression of the Pdk1 gene in both humans [91, 92] and mice [90] by binding to several HIF1 consensus binding sites (also known as hypoxia response elements). The important role of the HIF-1 signal pathway in bone development, modeling and remodeling is well documented. However, its role in osteocyte function remains unclear. Our findings showed that the expression of both Egln1 and Pdk1 were mechano-sensitive. Moreover, the increased expression of *Pdk1* after *Eno2* knockdown suggested a novel potential pathway for regulation of *Pdk1* by *Eno2*. Taken together, our study suggested that the HIF-1 signal pathway is also important for mechano-transduction in osteocytes, and Eno2 may be involved in the regulation of HIF-1 signal pathway in osteocytes. The role of HIF-1 signal pathway in the osteocyte function is worthy of further study.

II-5.3 *Previous studies about the role of Mxi1, Slc5a3, Bnip3, Eno2, and Higd1a in bone*

Besides Egln1 and Pdk1, other key DEGs were also found to play an important role in the bone metabolism.

Mxi1 encodes max-interacting protein 1, a transcription factor, was shown to suppress SOST transcription in human dermal fibroblasts in a recent study [93]. Sclerostin, which is encoded by SOST, a secretory protein that is specifically produced by osteocytes, suppresses osteogenesis by inhibiting WNT signaling [94, 95]. Recently, numerous studies have shown that sclerostin is a key determinant of the bone mass and a neutralizing antibody against sclerostin is currently being explored as a new therapeutic target for osteoporosis [96–99]. Interestingly, *Eno2* knockdown induced significant

expression decrease of *Mxi1* (**Fig.** II-7**A**). Meanwhile, significant correlation (Spearman's Rho, 0.67975; *P* value, 0.04397) between the expression of *Eno2* and *Mxi1* indicated a positive co-expression between *Eno2* and *Mxi1* (**Fig.** II-8). Therefore, our findings suggested a potential role of *Eno2* in the mechano-transduction for regulation of SOST, which is worthy of further study to confirm.

Sodium/myo-inositol transporter 1 (SMIT1), encoded by Slc5a3, is the major cotransporter for Myo-Inositol (MI), a crucial constituent and nutrient for living cells. $I(1,4,5)P_3$-mediated Ca^{2+} signaling, a pathway related to MI, was shown to modulate mechanical sensing in osteoblasts in a previous study [100]. SMIT1 knockout mice showed delayed embryonic bone formation, shortened adult long bones, a reduced bone mass, decreased numbers of osteoblasts, and osteoporosis-like microarchitecture, which suggests that SMIT1 plays essential roles in osteogenesis, bone formation, and bone mineral density [101].

B-cell lymphoma 2 (Bcl-2)/adenovirus E1B 19-kDa-interacting protein 3 (BNIP3), encoded by Bnip3, is a member of the apoptotic Bcl-2 protein family, which is involved in the atypical programmed cell death pathway through its modulation of the permeability state of the outer mitochondrial membrane [102]. The upregulation of BNIP3 was shown to contribute to the death of nucleus pulposus cells, which are embedded in intervertebral discs, during disc degeneration [103, 104]. Although most of these key DEGs (Mxi1, Slc5a3, Bnip3, Egln1, Pdk1) showed their important roles in the regulation of bone development, modeling and remodeling, the other key DEGs—specifically, Eno2, Higd1a and Ccng2, which are involved in energy metabolism, cell survival under stress and the regulation of cell cycle respectively—have not received enough attention in the field of bone research.

It is generally accepted that after differentiation, bone marrow mesenchymal stem cells (MSCs) become lineage-restricted and the terminal differentiated cell type (*e.g.* osteocyte) becomes irreversible. However, a previous study showed that after 24 hours of treatment with parathyroid hormone (PTH), the expression levels of *Kera* (osteoblast marker) and *E11* (early osteocyte marker)

were increased, whereas the expression levels of *Dmp1*, *Phex*, *Mepe* and *Sost* (mature osteocyte marker) were decreased in both mature IDG-SW3 osteocytes and the primary bone osteocytes *ex vivo*, indicating the loss of differentiation by osteocytes in response to PTH [105]. Their study also showed that some cell cycle-related genes (*e.g.* Rb1, Cebpa, Hpgd, Nupr1, and Bmp4) showed a decreased expression in response to PTH.

A previous study showed that adipogenic-differentiated cells from *ex vivo* human MSCs could be dedifferentiated and transdifferentiated into osteogenic or chondrogenic lineage cells, and this procedure is—at least in part—associated with genes associated with cell cycle arrest and progression [106]. Moreover, PTH has also been reported to induce the downregulation of Dmp1 in osteocytes *in vivo* [107]. Taken together, evidence showed the possible dedifferentiation of osteocytes, which may be associated with the regulation of cell cycle. The results of the present study showed the mechano-sensitive expression of Ccng2, which plays a role in the negative regulation of cell cycle progression.

HIG1 domain family 1A (HIGD1A), which is encoded by Higd1a, is a protein that promotes mitochondrial homeostasis and the survival of cells under stress by inhibiting cytochrome C release and caspase activity [108, 109]. It plays a very important protective effect that saves organs like the heart and brain from hypoxia-related disease [109]. Decreased expression of *Higd1a* by *Eno2* knockdown and correlated expression between them might indicate that *Eno2* may be involved in the hypoxic response of osteocytes.

Gamma-enolase, encoded by Eno2, is a conserved glycolytic enzyme that catalyzes the formation of phosphoenolpyruvate from 2-phosphoglycerate, which generates ATP during glycolysis. A recent study showed that alpha-enolase regulates the AMPK/mTOR pathway, which plays important roles in bone metabolism [110–112], via the concentration of ATP in colorectal cancer cells [113]. Notably, *Eno2* was significantly increased in both human periodontal ligament (PDL) cells with compressive stress [114] and murine osteoblasts with thapsigargin treatment (ER stress) [115].

II-5.4 *Mechano-transduction in osteocytes possibly regulates the innervation of bone*

Although there have been numerous studies of the key DEGs in the field of bone research, the biological function of these key DEGs in osteocytes has been poorly studied. Thus, to investigate the biological function of the key DEGs, we selectively downregulated the hub gene of the final PPI network using siRNA.

Eno2 knockdown results in a significant increase in the expression of *Gap43* (**Fig.** II-7**A**). Gap43 encodes the neuromodulin that plays a role in axonal and dendritic filopodia induction. Neuromodulin has been identified in the extracellular vesicles (EVs) derived from human MSCs [116]. Furthermore, the rapid expansion of a dense network of sensory nerve fibers is observed during fracture repair in the periosteum of adult rodents. Thus, it is possible that the induction of nerve fibers is subject to regulation by Gap43 in EVs secreted by osteocytes [117–119]. Interestingly, in the *in vitro* experiment, the expression of Eno2 and Gap43 did not show a significant correlation under 2.5 dyn/cm2, while they were highly correlated (**Fig.** II-8) under extremely high mechanical force (50 dyn/cm2). The co-expression of Eno2 and Gap43 under a pathological force load is consistent with our hypothesis that osteocytes may have able to induct the expansion of nerve fibers under serious injury. However, further physiological studies are necessary to prove this hypothesis. In recent years, there is increasing evidence to support the role of EVs in bone remodeling, and that bone marrow stem cells, osteoblasts, osteoclasts, and osteocytes can communicate with one another and even other types of organs/cells via EVs [120]. Notably, mechanical stimulation has been shown to upregulate the production of EVs in osteocytes, which could enhance bone formation [121], while the muscle cells secreted myostatin downregulate the miR-218 (a microRNA) in EVs derived from osteocytes, which inhibits osteoblastic differentiation [121]. Moreover, previous studies have suggested that some of the regenerative effects are mediated by EVs derived from MSCs [122–124].

II-6 Conclusions

In the present study, we screened out and primarily validated some candidate genes that showed extremely mechano-sensitive expression levels. The results indicated the important role of these genes

in osteocytes in relation to sensing, recognizing and the differential responses to different types of mechanical stimuli. We also reviewed the previous studies of these genes in the field of bone research. Our research raised a number of questions.

Unloading [125], aging [126], compressive force [127], and osteoporosis [128] could induce the death of osteocytes, while could Higd1a promote osteocyte survival under those conditions? Is it possible that osteocyte-secreted EVs are important for regulating bone metabolism and crosstalk with other organs? Do the cell cycle-related genes play a role such as triggering dedifferentiation of osteocytes? How exactly do the key DEGs that we screened out regulate the osteocyte functions? What is the exact mechanism of the mechano-sensitive expression of these key DEGs? Some of these questions have touched on some current topics in the field of bone research. Other questions are related to genes that have not been completely studied; thus, their relationship to bone remains unclear. The authors believe that exploring and finally answering these questions could improve our understanding of mechano-transduction in osteocytes and may lead to the development of new therapeutic agents for bone diseases.

Chapter III

Energy Metabolism may Regulate Gap-Junctional Intercellular Communications and Its Possible Biological Functions in the Bone Metabolism

III-1 Responding to mechanical stimuli in osteocytes may subject to the regulation of energy metabolism by hypoxia signaling pathway

Since oxygen acts as a final electron acceptor in oxidative phosphorylation for energy production, sophisticated systems for responding to changes in oxygen concentration were developed in aerobic organisms under the evolution pressure. Hypoxia-inducible factor (HIF) plays a central role in the adaptive regulation of energy metabolism, by determining fate of pyruvate to be metabolized to lactate, remodeling mitochondria, and regulation of lipid metabolism in hypoxia [129]. Our bioinformatic analysis and followed validation experiments in **Chapter II** suggested that hypoxia signaling pathway and energy metabolism related genes (Eno2, Higd1a, and Ccng2) may play the crucial role for the differential response to different types of mechanical stimulation in osteocytes. Our results showed that the expression of Egln1 was mechanical sensitive (**Fig.** II-6). Egln1 encodes a prolyl-4-hydroxylase (PHD) enzyme — a type of proteasome — that degrades the hypoxia-inducible transcription factor (HIF)-1α by hydroxylation and results in the post-translational regulation of HIF. HIF1α impacts the expression of sclerostin, which showed by a recent proposed model [130] of a PHD2-HIF1α-SIRT1-sclerostin-WNT/β-catenin connections in response to changes in HIF levels in osteocytic lacunae.

III-2 Regulation of gap-junctional intercellular communication by hypoxia signaling is well-documented in other cells type but not osteocytes

Conductance and permeability of GJIC could be increased by dephosphorylation of Cx43, which in turn is involved in the spread of ischemia/reperfusion injury-induced hypoxia [131]. Dephosphorylation and redistribution of Cx43 were observed as an early sign of hypoxia-induced

cardiac injury [132]. Preserving the phosphorylation status of Cx43 from the hypoxia by diltiazem could protect the heart by a decrease of the risk of reentrant arrhythmia via inhibiting the disturbance of intercellular communication [133]. Hypoxia decreased Cx43 protein and conduction velocity in rat ventricular myocytes [134], but increased Cx43 protein in rat carotid body, petrosal ganglion, and vascular smooth muscle cells [135, 136]. Indeed, GJIC capacity was increased in vascular smooth muscle cell by using the FRAP technique [135]. The findings above suggested that the expression of Cx43 regulated by hypoxia may be lineage-specific. In the research field of bone, *Bglap-cre*; *Hif1a* cKO mice showed a low bone mass phenotype [137], whereas *Hif1a* cKO mice do not [138], and the only deletion of both *Hif1a* and *Hif2a* showed a skeletal phenotype [82]. Those findings suggested the lineage-specific necessity for a particular HIF-α gene in bone cells. However, to the author's acknowledge, there is no investigation of the Cx43 expression in osteocytes under hypoxia.

Osteocytes trapped in the bone matrix are more susceptible to hypoxia than osteoblasts and osteoclasts. Consideration of discussions above and findings that are shown in **Chapter II**, hypoxia regulated expression level and phosphorylation status of Cx43 may be a possible mechanism for the osteocyte differentiation-induced changes of gap-junctional intercellular communication capacity observed in our previous work [65]. There is, however, no direct evidence to support this hypothesis. This hypothesis is worthy of further study to verify, since oxygen sensing in bone is fundamentally necessary for skeletal health, is altered in pathological states, and can be pharmacologically manipulated [139].

III-3 Possible interactions between biorhythm and energy metabolism

Notably, regulation of circadian rhythm (GO:0072452) was a significant enriched term for the MLO-Y4 cells responding to fluid flow (**Appendix Fig. 2**). Biological rhythms exert important regulatory control over an organism's physiology, behavior, and development. Biological rhythms are particularly visible as the daily metabolic fluctuations that are attributed to the central circadian clock. In mammalian species, the formation of enamel (striae of Retzius) and bone growth (the periodic

formation of lamellae) are both periodic processes that are highly associated with all the common aspects of life-history timing, i.e., the age of sexual maturity and lifespan, and mass characteristics, i.e., neonatal body mass and adult brain weight, together with the basal and specific metabolic rates [140–142]. The number of daily events between adjacent striae of Retzius is termed the repeat interval (RI). RI is a manifestation of a fundamental metabolic rhythm, and is significantly associated with primate tissue, organ, and body mass; most of the correlations between RI and the mass of body, fat-free body, brain, heart, lung, kidney, liver, digestive tract, stomach, intestine, spleen, visceral, adipose, and basal metabolic rate are significant at the 0.01 level [142]. Due to its pivotal role, Bromage et al. named this period Havers-Halberg oscillation (HHO) [140].

HHO governs the biorhythm of body development at the tissue level, and it should be supported at the cellular level. Some studies have shown that a lack of clock genes, such as Bmal1 or Per, can affect bone mass [19–21]. Moreover, a recent study demonstrated that Circadian Locomotor Output Cycles Kaput (Clock) is a transcriptional activator of the protein disulfide isomerase family A member 3 (PDIA3) gene, which in turn protects osteoblasts from disordered apoptosis and osteogenesis; the study indicated that the biorhythm plays an important role in osteoblast function [143]. Furthermore, recent studies have shown that the circadian clock control impacts numerous aspects of energy metabolism [144].

III-4 An “energy-saving” strategy hypothesis for the future studies

Since the intake and transport capacity of energy is limited, the biorhythm might have a functional role to temporospatially orchestrate the energy consumption. **Fig.** III-1 shows one hypothesized example of how this sequence of energy consumption optimizes the efficiency of energy consumption. This optimization might be crucial, especially for bone, which requires a great deal of energy support, but in which the support channel is limited by its structure. Our previous work [65] using *ex vivo* chick calvariae showed that not all osteocytes have observable gap junctional intercellular communication (GJIC). Among all 93 valid experimental target osteocytes, only 25 cells showed observable GJIC. In

these 25 cells, this study demonstrated two types of GJICs in the development of mature osteocytes in chicks, passive transduction (low GJIC osteocyte) and active transduction (high GJIC osteocyte). Based on this finding, we hypothesize that there is a pattern in which high GJIC osteocytes function as a control node that maintains a high GJIC to allow a quick response to stimuli, to activate the surrounding osteocytes, and maintain the coordination of the osteocyte biorhythm (**Fig.** III-2). This finding is also consistent with our hypothesis in **Fig.** III-1, that an unknown mechanism causes the peak in energy consumption to occur at a different time point for each individual cell, to optimize the energy consumption via the biorhythm (**Fig.** III-1).

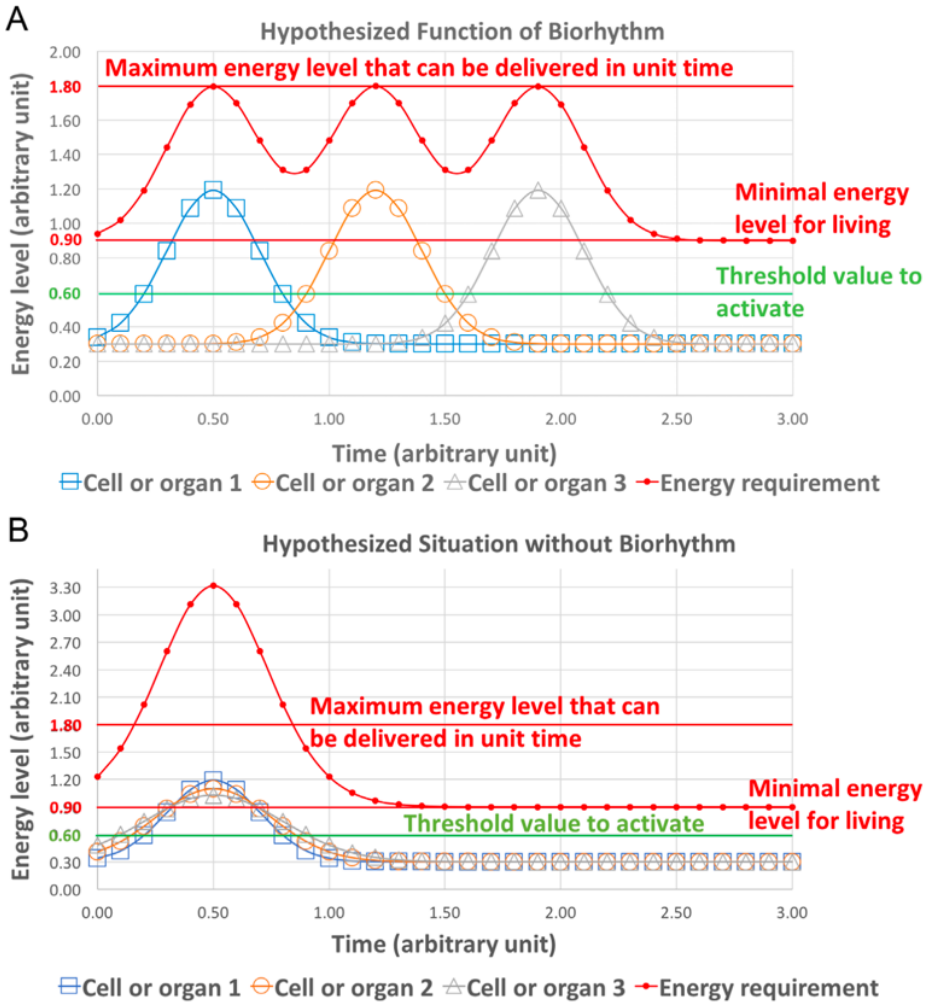

Fig. III-1. The hypothesized function of biorhythm.
(**A**) Coordination of the biorhythm results in a smooth curve of energy requirement. (**B**) A lack of biorhythm coordination results in a sharp curve of energy requirement.

Cx43, the predominant gap junction protein in bone, may play an important role in this unknown mechanism. Cx43 deficiency results in a significant decrease in bone formation but increases the

sensitivity to mechanical loading [145]. Our hypothesis can partially explain this paradox. According to our hypothesis, Cx43 deficiency breaks the coordination of the biorhythm in osteocytes, resulting in a sharp curve of energy requirement (**Fig.** III-1**B**). As **Fig.** III-1**B** indicates, this can induce insufficient energy support, which, subsequently, might cause osteocytic osteolysis or the apoptosis of osteocytes to reduce the bone mass. As **Fig.** III-1**B** shows, a more synchronized response may be caused by the damaged coordination of the biorhythm, which causes the bone to respond to the stimuli more acutely. Our hypothesis lacks rigorous evidence; however, we are currently performing further investigational studies.

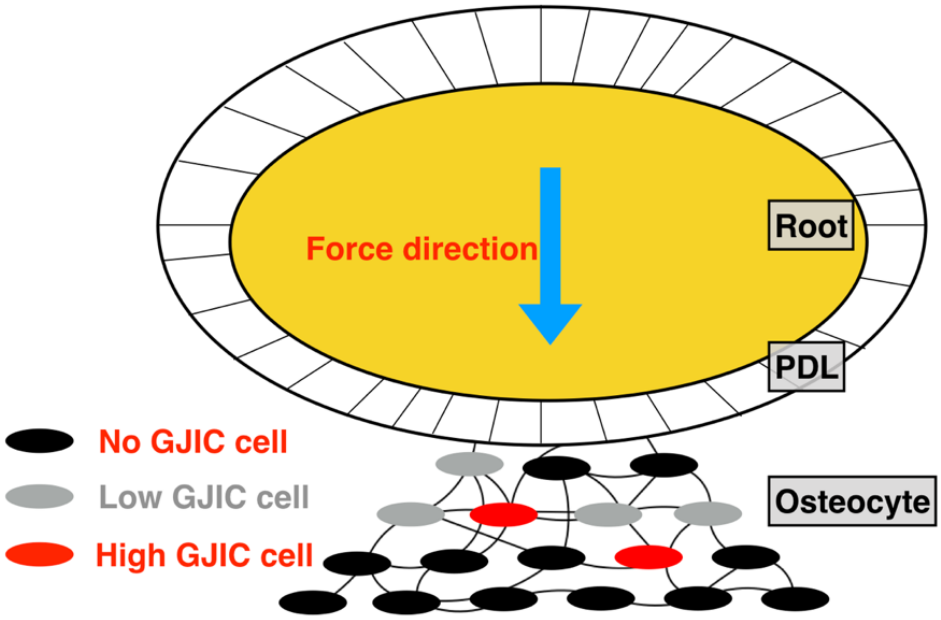

Fig. III-2. The control node pattern.
Few osteocytes maintain high activity to sense stimuli and activate the surrounding osteocytes. PDL: periodontal ligament; GJIC: gap junctional intercellular communication.

In summary, the cell biorhythm, which assigns a different timing to the peak energy consumption of individual cells, appears to be a possible “energy-saving” strategy in response to energy support limitations which could greatly improve the efficiency of energy utilization. However, there is currently no direct evidence to support this hypothesis. If this hypothesis could be verified, we may eventually find a therapeutic window through which we can impact the temporospatial pattern of energy metabolism in order to control the biological events in our body system, such as to accelerate tooth movement in orthodontics or to slow osteoporosis.

Acknowledgements

First of all, I would like to express my sincere gratitude to Research Fellowships of Japan Society for the Promotion of Science for doctoral students (DC2), for financial support. The DC2 scholarship [19J1190611] is crucial for me to complete this work.

Utmost appreciation goes to Professor Hiroshi KAMIOKA for his guidance, support, ideas, motivation, and patience during the entire studies. I could not have any achievements without his supervision and taught.

My special thanks due to Dr. Yoshihito ISHIHARA for his generous advice, assistance, encouragement, patience, and dedicated support during the entire period of my doctoral course. Without his help, completing my doctoral course would be difficult.

I am also grateful to Dr. Naoya ODAGAKI and Dr. Ei EI HSU HALING who gave brilliant discussions to spirit me, technical assistance for almost all of my experiments, and friendship to save me from bored trifles.

I thank Dr. Yoshitaka KAMEO, Department of Biomechanics, Research Center for Nano Medical Engineering, Institute for Frontier Medical Sciences, Kyoto University, for fruitful discussions on the mathematical model of simple diffusion. I thank Dr. Takanori ISHIKAWA, Dr. Mitsuhiro HOSHIJIMA, Dr. Tomoyo TANAKA, Dr. Mana HASHIMOTO, Dr. Masahiro NAKAMURA, Dr. Satoru HAYANO, and Dr. Noriaki KAWANABE for their cooperation in this work.

Greatest pleasure goes to acknowledge the efforts of many people who directly or indirectly gave their support, guidance, motivation, cooperation, and understanding for this work.

Finally, I wish to thank my wife, Yao Weng, who saw too much of the back of my head and take care of my life as I looked at the computer screen while I was coding, processing data, and revising the thesis before the deadline. I could not live without her taking care of my daily life. My wife's tolerance is best described as remarkable. Great thanks to my parents for their love and encouragement.

Appendix

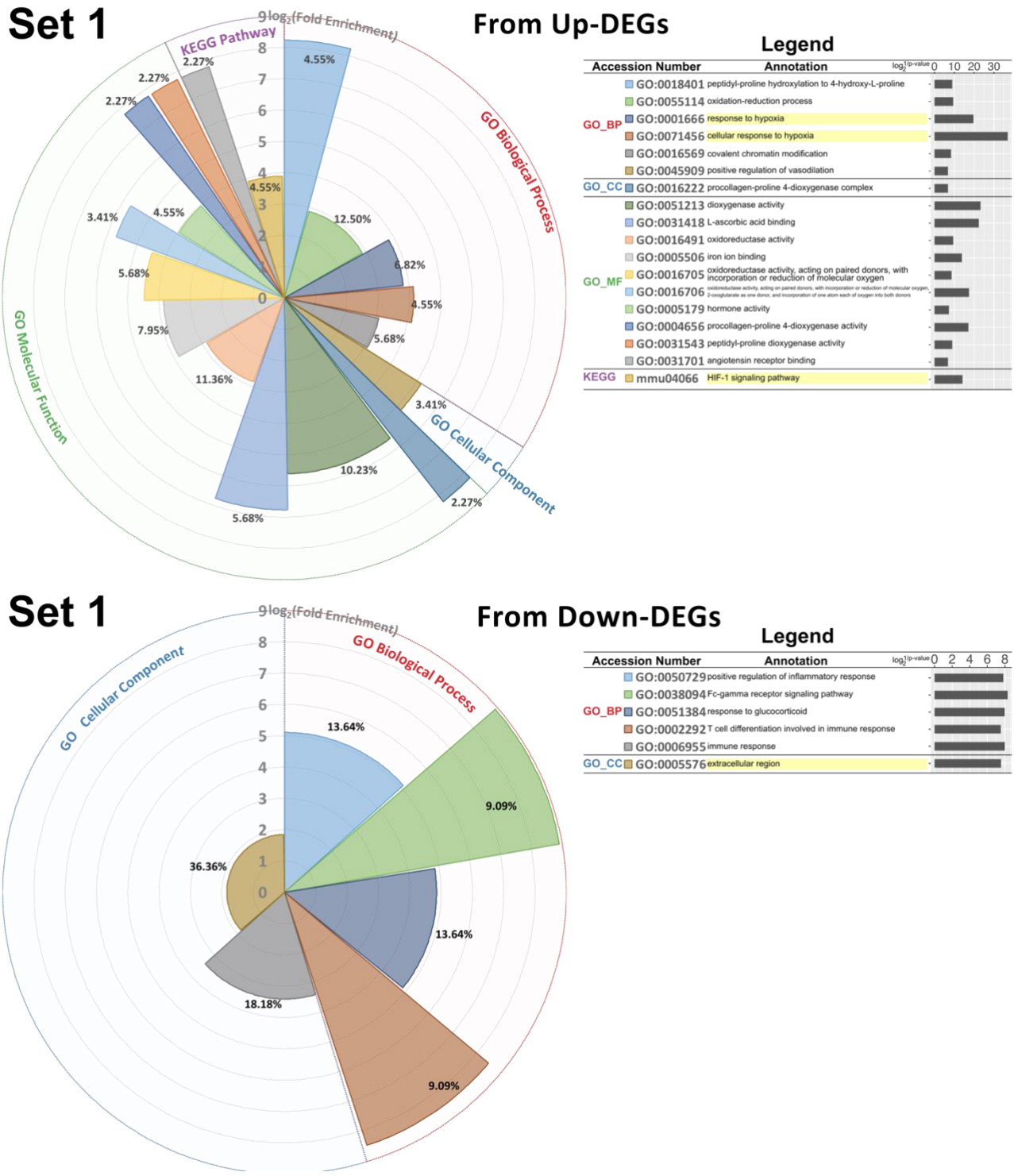

Appendix Fig. 1. The complete list of the functional enrichment of Set1.
The height of each slice represents the log2 value (fold enrichment). The radian of each slice represents the percentage of DEGs for the corresponding term to all queried DEGs; the exact percentage is shown by the label of each slice. The common terms between Set1 and Set2 are in yellow highlight.

Appendix Table 1. The complete list of DEGs of Set1.

No.	symbol	logFC	AveExpr	t	P.Value	adj.P.Val
1	P4ha2	1.111701	9.445893	25.681079	0.000000	0.002566
2	Stc1	1.845347	8.828050	27.455337	0.000000	0.002566
3	Cd53	-0.769892	6.394318	-17.261204	0.000002	0.009355
4	Loxl2	1.001999	9.434474	17.897610	0.000002	0.009355
5	Elovl3	-0.828730	6.535543	-18.241936	0.000002	0.009355
6	Dixdc1	0.760056	8.032514	17.310900	0.000002	0.009355
7	Ak3l2-ps	1.807144	10.448745	16.296584	0.000003	0.011310
8	Wdr12	-0.610081	8.483593	-15.495880	0.000004	0.013369
9	Clec4d	-0.852963	6.341690	-14.740132	0.000005	0.015058
10	Higd1a	1.196394	8.747896	14.602376	0.000006	0.015058
11	Tnf	-0.655880	8.933006	-14.398007	0.000006	0.015058
12	Arl11	-0.650266	7.233297	-12.259864	0.000016	0.024146
13	Plod2	0.604668	11.219803	12.469037	0.000015	0.024146
14	S100b	-0.774873	10.787502	-11.953004	0.000019	0.024146
15	Desi2	0.659538	5.978314	12.125264	0.000017	0.024146
16	Mir18	-0.604418	7.793172	-11.646960	0.000022	0.024146
17	Bnip3	0.943860	11.320845	11.816898	0.000020	0.024146
18	Plekha2	0.653125	9.486824	11.841791	0.000020	0.024146
19	Gdap10	0.833994	7.275106	10.740183	0.000035	0.030944
20	Nadk2	0.609791	8.913376	10.407479	0.000042	0.030944
21	Pfkl	0.687789	11.552565	9.614974	0.000066	0.037596
22	Gm10581	0.610123	8.800435	9.580708	0.000067	0.037596
23	Gsta1	-0.615249	7.347496	-9.308304	0.000079	0.038725
24	Gm11448	-0.707246	5.842115	-9.171759	0.000086	0.038725
25	Prnd	-0.908829	7.452361	-9.153374	0.000087	0.038725
26	Gys1	0.621935	11.740936	9.084730	0.000091	0.038725
27	Mxi1	0.591334	9.404675	8.740655	0.000114	0.041031
28	Gm29609	0.801754	4.929033	8.694705	0.000117	0.041031
29	Gpr35	1.030402	9.220791	8.688542	0.000118	0.041031
30	Il1rn	-0.759685	7.600734	-8.660280	0.000120	0.041263
31	Apln	1.160339	10.096541	8.487569	0.000134	0.043483
32	Rpp40	-0.951329	7.618741	-8.238606	0.000159	0.043673
33	Ppp1r3c	0.717169	6.038492	8.235723	0.000160	0.043673
34	P4ha1	0.884001	10.948692	8.197429	0.000164	0.043673
35	Gm16439	0.790546	12.046383	8.012809	0.000186	0.043713
36	Vmn2r31	0.646847	4.396340	7.992132	0.000189	0.043713
37	Calb2	-0.660328	9.092259	-7.958735	0.000193	0.043997
38	B130024G19Rik	0.787383	6.890117	7.857391	0.000208	0.044634
39	Pinx1	-0.602153	9.348127	-7.827214	0.000212	0.044748
40	Tbl2	0.611673	9.614306	7.809851	0.000215	0.044748
41	Ccl3	-1.357949	10.528024	-7.643160	0.000243	0.045120
42	Gpr84	-1.976375	7.933665	-7.559595	0.000258	0.045776
43	Slc5a3	0.643807	8.803569	7.553362	0.000259	0.045776
44	Fyb	0.639666	7.693870	7.512906	0.000267	0.046255
45	Egln1	0.658145	10.755716	7.401471	0.000290	0.046655
46	S100a8	-0.648477	9.058614	-7.077709	0.000372	0.051425

Appendix Table 1. The complete list of DEGs of Set1. (Continuous)

No.	symbol	logFC	AveExpr	t	P.Value	adj.P.Val
47	Il1r1	0.606376	9.976237	6.721732	0.000494	0.054916
48	Tet2	0.781551	8.620226	6.645532	0.000525	0.054916
49	Kdm4b	0.643248	9.079579	6.593200	0.000548	0.055579
50	Col6a3	0.672395	8.936667	6.394684	0.000647	0.058074
51	Pdk1	0.684693	9.496543	6.206159	0.000760	0.061480
52	Mcpt8	-0.976649	6.608935	-5.958875	0.000944	0.063907
53	Eno2	0.848390	10.134684	5.906643	0.000990	0.064863
54	Timm8a1	-0.625585	9.020301	-5.856528	0.001035	0.066226
55	Arrb1	1.130398	10.052821	5.803590	0.001086	0.066767
56	Rcor2	0.856405	9.037043	5.728495	0.001163	0.067396
57	Igsf10	0.695619	7.603592	5.675831	0.001221	0.068125
58	Kdm3a	0.619565	10.040271	5.621968	0.001283	0.068334
59	Gm22951	0.608926	6.447490	5.601916	0.001308	0.068458
60	Kdm5b	0.707786	7.828428	5.469720	0.001481	0.072113
61	Ankrd37	0.625706	7.325801	5.459825	0.001495	0.072529
62	Crct1	-1.301743	8.699580	-5.428567	0.001540	0.072874
63	Adm	0.951259	9.901415	5.393882	0.001592	0.073264
64	Obox4-ps28	0.728957	5.441881	5.376282	0.001619	0.073349
65	Egln3	0.810820	7.283467	5.288737	0.001761	0.074673
66	Wdr78	0.668250	7.216704	5.263285	0.001806	0.075444
67	Adamts5	0.671705	10.312684	5.256979	0.001817	0.075444
68	Obox4-ps27	0.665251	5.166201	5.225079	0.001874	0.075661
69	Clec4e	-1.502072	8.432181	-5.115007	0.002089	0.078237
70	Olr1	-0.857069	5.762024	-5.063951	0.002198	0.079362
71	Ccng2	0.904061	9.339020	4.966961	0.002423	0.081981
72	Malat1	0.613261	11.376503	4.756010	0.003010	0.087642
73	Obox4-ps33	0.727838	5.541774	4.741886	0.003054	0.088010
74	Cml5	-1.181827	8.025122	-4.689162	0.003228	0.089418
75	Sned1	0.835188	9.819715	4.683965	0.003246	0.089551
76	Gch1	-0.707592	7.893482	-4.674708	0.003277	0.089551
77	Agt	0.811278	7.450314	4.584922	0.003604	0.091491
78	Bglap2	-0.788049	8.581267	-4.536552	0.003796	0.093622
79	Nxph4	0.603041	9.181374	4.531910	0.003815	0.093745
80	Gm22510	0.636536	4.257179	4.494109	0.003973	0.094538
81	Ndufa4l2	1.733009	9.820684	4.441157	0.004207	0.096441
82	Gm9847	-0.716854	7.856231	-4.369318	0.004551	0.098373
83	Dubr	0.791875	9.847323	4.335955	0.004721	0.099655

logFC, log2-fold-change
AveExpr, Average log2-expression for the probe over all arrays and channels
t, moderated t-statistic
P.Value, raw p-value
adj.P.Val, Benjamini and Hochberg FDR adjusted p-value

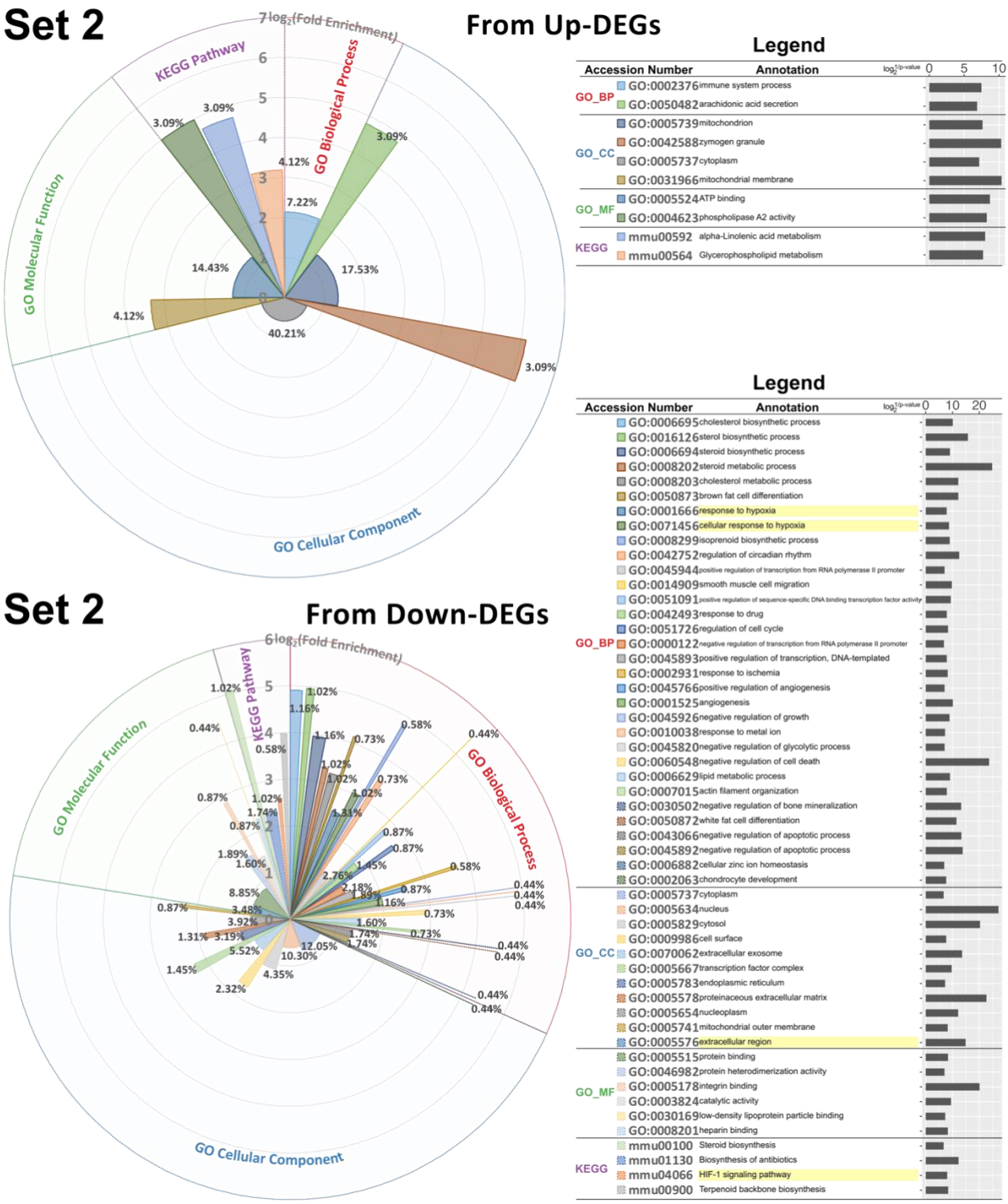

Appendix Fig. 2. The complete list of the functional enrichment of Set2.
The height of each slice represents the log2 value (fold enrichment). The radian of each slice represents the percentage of DEGs for the corresponding term to all queried DEGs; the exact percentage is shown by the label of each slice. The common terms between Set1 and Set2 are in yellow highlight.

Appendix Table 2. The complete list of DEGs of Set2.

No.	symbol	logFC	AveExpr	t	P.Value	adj.P.Val
1	Hmgcs1	-1.270054	9.594938	-28.549548	0.000000	0.001929
2	Olfm1	-1.206775	7.553325	-26.692825	0.000000	0.001929
3	Pvrl2	1.079300	6.336075	23.094601	0.000000	0.002289
4	Ldlr	-0.998065	9.324736	-21.359875	0.000001	0.002830
5	Hnrnpdl	-1.065790	8.093611	-18.857653	0.000001	0.003559
6	Mfsd6	1.065667	8.468552	19.112237	0.000001	0.003559
7	Mettl20	1.237863	6.834810	18.206070	0.000002	0.003559
8	Pycr1	1.104816	8.900821	17.749307	0.000002	0.003649
9	Rgs2	-1.105533	8.300161	-17.243856	0.000002	0.003997
10	P2rx5	-0.917475	6.792430	-17.000696	0.000003	0.004037
11	Ahi1	0.706026	7.874527	16.506104	0.000003	0.004486
12	Cyp51	-1.053936	8.870407	-16.049120	0.000004	0.004964
13	Slc6a8	-0.771485	9.120500	-15.279891	0.000005	0.005894
14	Rbbp6	-0.599136	7.031282	-14.839075	0.000006	0.006513
15	Ndrg1	-0.921371	8.567137	-14.499505	0.000007	0.006513
16	Klra2	1.481714	7.124013	14.567862	0.000006	0.006513
17	Zfp326	-0.752167	9.155780	-14.117413	0.000008	0.006513
18	Mt1	-1.481559	12.493230	-14.090741	0.000008	0.006513
19	Msmo1	-0.770815	9.468998	-13.934331	0.000008	0.006513
20	Enah	-0.704645	9.657136	-14.505989	0.000007	0.006513
21	Slc48a1	0.752006	10.315153	13.987282	0.000008	0.006513
22	Pspc1	-1.225596	8.545886	-14.073544	0.000008	0.006513
23	Lims2	-0.622231	7.553070	-13.801048	0.000009	0.006653
24	Sox9	-0.656995	7.039550	-13.714731	0.000009	0.006672
25	Sdpr	0.794754	9.262003	13.512681	0.000010	0.006877
26	Srsf6	-0.609292	10.160127	-13.423682	0.000010	0.006877
27	Leprotl1	0.619314	10.654530	13.457657	0.000010	0.006877
28	Ptpn22	0.778693	7.838437	13.297926	0.000011	0.007052
29	Syncrip	-0.689039	8.198289	-13.171206	0.000012	0.007245
30	Acad11	0.618460	7.219765	12.920289	0.000013	0.007882
31	Denr	-0.942962	7.178465	-12.828858	0.000013	0.007959
32	Tjp2	-0.808669	7.266700	-12.722980	0.000014	0.007959
33	Ypel3	0.662817	7.957496	12.731322	0.000014	0.007959
34	Hif1a	-0.730023	5.153147	-12.540642	0.000015	0.008021
35	Dhcr24	-0.796403	9.198170	-12.482112	0.000016	0.008021
36	Col3a1	-1.617095	7.366086	-12.418890	0.000016	0.008021
37	Pcmtd2	0.689566	7.005639	12.396386	0.000016	0.008021
38	Pes1	-0.809870	6.659549	-12.223154	0.000018	0.008021
39	Gm38481	-0.955462	8.809473	-12.217018	0.000018	0.008021
40	Tcf7	-0.726473	6.593888	-12.341489	0.000017	0.008021
41	Atp6v1a	-0.609323	10.442556	-12.175309	0.000018	0.008021
42	Bnip3	-1.767144	9.779513	-12.244197	0.000018	0.008021
43	Itgb2	-1.041295	7.579125	-11.857825	0.000021	0.008369
44	Elp4	-0.597154	4.966311	-11.853219	0.000021	0.008369
45	Kif22	0.672811	8.689557	11.924469	0.000021	0.008369
46	Tpd52	0.604224	8.707371	11.696728	0.000023	0.008794

Appendix Table 2. The complete list of DEGs of Set1 (Continuous)

No.	symbol	logFC	AveExpr	t	P.Value	adj.P.Val
47	Timp2	-0.742469	8.916902	-11.608331	0.000024	0.008794
48	Strbp	0.797616	6.994837	11.548012	0.000025	0.008794
49	Bpgm	0.793566	6.773778	11.392371	0.000027	0.009362
50	Nov	-0.910994	11.281318	-11.220281	0.000029	0.009709
51	Camk1d	-0.620935	7.448730	-11.093236	0.000031	0.009709
52	Mapre2	-0.599379	8.325383	-10.998286	0.000033	0.009902
53	Scmh1	0.593763	8.012899	10.808805	0.000036	0.010150
54	Hk2	-0.838586	10.251280	-10.833452	0.000036	0.010150
55	Prkar1b	0.733744	6.083773	10.737814	0.000038	0.010150
56	Txnl1	-0.707884	8.445088	-10.732557	0.000038	0.010150
57	B3galnt2	0.617403	8.542699	10.569443	0.000041	0.010403
58	Tmem158	-0.982161	9.051729	-10.542175	0.000042	0.010403
59	Nedd4l	-0.781726	9.593431	-10.535701	0.000042	0.010403
60	Nucb2	0.708241	10.652435	10.511228	0.000043	0.010403
61	Aldh1l1	-0.807749	6.851576	-10.493118	0.000043	0.010403
62	Limch1	-0.613251	6.760628	-10.475111	0.000043	0.010403
63	Lancl2	-0.590958	10.081333	-10.325618	0.000047	0.010949
64	Rnd3	-0.672226	6.761181	-10.233876	0.000050	0.011043
65	Abcc1	0.620923	11.400596	10.221768	0.000050	0.011043
66	Wasf1	-0.667982	8.946808	-10.104916	0.000053	0.011156
67	Vav3	-1.225292	7.609063	-10.080810	0.000054	0.011156
68	Il18	0.891595	8.950818	10.008377	0.000056	0.011300
69	Akap2	-0.889592	9.408113	-9.730436	0.000066	0.012187
70	Rgcc	-2.092422	8.367891	-9.690734	0.000068	0.012233
71	Tnfsf11	-0.623400	5.794296	-9.701321	0.000067	0.012233
72	Mtch2	-0.600179	8.178485	-9.672137	0.000069	0.012233
73	Srsf3	-0.692856	9.133807	-9.641404	0.000070	0.012233
74	Enpp3	-0.629035	7.058180	-9.623135	0.000071	0.012233
75	Tnfaip6	-0.770394	7.956909	-9.570123	0.000073	0.012267
76	Mt2	-0.927531	12.956585	-9.548019	0.000074	0.012267
77	Colec12	-0.705973	9.904561	-9.542734	0.000074	0.012267
78	Ttc23	0.700144	7.186284	9.423675	0.000080	0.012791
79	Sqle	-0.930640	10.032101	-9.249657	0.000088	0.013610
80	Stard4	-0.719167	7.207666	-9.139710	0.000095	0.013622
81	Dnaja4	0.599086	8.367533	9.148567	0.000094	0.013622
82	Grem1	-0.672286	11.644034	-9.055683	0.000100	0.013802
83	Srsf7	-0.665201	10.480860	-8.903660	0.000110	0.014389
84	Mapk12	0.796256	8.097556	8.686958	0.000126	0.015215
85	Thbs2	-1.186038	9.437636	-8.636715	0.000130	0.015261
86	Ivns1abp	-0.919409	6.392746	-8.630236	0.000131	0.015261
87	Wisp1	-0.656882	7.288699	-8.602244	0.000133	0.015288
88	Acsl1	-0.729200	8.752540	-8.507171	0.000142	0.015701
89	Lifr	-0.867505	4.987179	-8.474433	0.000145	0.015806
90	Crem	1.123207	6.956060	8.453370	0.000147	0.015871
91	Dopey2	0.593179	6.520288	8.401293	0.000152	0.016115
92	Higd1a	-1.007932	7.316636	-8.298127	0.000163	0.016809

Appendix Table 2. The complete list of DEGs of Set1 (Continuous)

No.	symbol	logFC	AveExpr	t	P.Value	adj.P.Val
93	Alg12	0.628524	7.610615	8.288902	0.000164	0.016809
94	Runx2	-0.801596	8.837495	-8.196176	0.000175	0.017184
95	1190002N15Rik	-0.670227	8.019394	-8.189126	0.000175	0.017188
96	Ak4	-1.233838	5.920749	-8.173518	0.000177	0.017188
97	Ogt	0.659257	6.765381	8.161026	0.000179	0.017217
98	Ttyh2	-0.862585	9.223090	-8.135191	0.000182	0.017268
99	Acat2	-0.908750	8.950861	-8.106873	0.000186	0.017268
100	Baiap2	-0.630115	6.587112	-8.109661	0.000185	0.017268
101	Pyhin1	2.309438	4.747007	8.091887	0.000187	0.017268
102	Tfec	0.612019	6.761528	8.066559	0.000191	0.017371
103	Rbm47	-0.837280	6.631234	-8.061826	0.000191	0.017371
104	Hopx	-0.903066	6.961767	-8.038721	0.000194	0.017579
105	Hivep2	-0.996103	7.545232	-8.024812	0.000196	0.017583
106	Pnpla7	0.715801	8.067074	8.003510	0.000199	0.017669
107	Angptl6	0.871866	8.796633	7.936966	0.000209	0.017857
108	Nnmt	0.921100	8.309684	7.927622	0.000210	0.017857
109	Lima1	-0.591565	7.566470	-7.943615	0.000208	0.017857
110	Mxi1	-0.771310	7.832564	-7.824198	0.000226	0.018063
111	Cox6a2	1.017008	8.275133	7.836182	0.000224	0.018063
112	Aldh3a1	-1.303479	7.721754	-7.833157	0.000225	0.018063
113	Ndc1	0.607584	10.172533	7.705800	0.000246	0.018642
114	Fabp4	-0.745360	6.316592	-7.699038	0.000247	0.018669
115	Prss23	-0.940958	9.169220	-7.618186	0.000262	0.019305
116	Sft2d2	0.608254	7.542996	7.585497	0.000268	0.019335
117	Chst11	-1.246676	7.645452	-7.596803	0.000266	0.019335
118	Rab11fip5	0.748177	7.835735	7.589918	0.000267	0.019335
119	Ntn1	-0.743795	10.280556	-7.538257	0.000278	0.019446
120	Cul3	-0.642223	6.841378	-7.412725	0.000305	0.020361
121	Pmvk	-0.735298	7.928841	-7.393288	0.000309	0.020532
122	Chid1	0.618576	8.044015	7.380818	0.000312	0.020589
123	Ascc2	0.676314	7.178390	7.304065	0.000330	0.021558
124	Serpind1	0.622388	7.034931	7.264786	0.000340	0.021567
125	Cxcl9	0.717198	9.386714	7.265561	0.000340	0.021567
126	Slc2a1	-0.827979	9.879655	-7.289538	0.000334	0.021567
127	Chchd10	0.816110	11.993325	7.277062	0.000337	0.021567
128	Pcbp2	-0.620419	9.481075	-7.120004	0.000380	0.022706
129	Nfatc1	-0.666014	7.464186	-7.107173	0.000384	0.022747
130	Lox	-0.869796	12.076404	-7.082035	0.000391	0.022945
131	Procr	1.005325	11.094118	7.055542	0.000399	0.023172
132	Lss	-0.726247	6.138091	-6.997060	0.000418	0.023395
133	Fam13b	-0.817595	8.886283	-6.941084	0.000436	0.023825
134	5031439G07Rik	-0.616772	8.820066	-6.919404	0.000444	0.023969
135	Hsd17b7	-0.977719	7.858487	-6.815653	0.000482	0.025002
136	Zbp1	0.837553	9.468791	6.612288	0.000567	0.026827
137	C920025E04Rik	0.931546	7.469641	6.573994	0.000585	0.027075
138	Slc43a3	0.674038	8.549560	6.529573	0.000607	0.027381

Appendix Table 2. The complete list of DEGs of Set1 (Continuous)

No.	symbol	logFC	AveExpr	t	P.Value	adj.P.Val
139	Phyhd1	0.901698	6.474421	6.516764	0.000614	0.027503
140	Gabarapl1	0.689106	9.379388	6.502112	0.000621	0.027557
141	Macrod1	0.634992	7.761291	6.483170	0.000631	0.027830
142	Lactb	-0.600314	7.610973	-6.456121	0.000645	0.027951
143	Pla2g12a	0.687077	9.666991	6.441541	0.000653	0.028155
144	Il18bp	0.642095	8.580216	6.332966	0.000715	0.029061
145	Afp	0.639564	3.837779	6.350455	0.000705	0.029061
146	Coasy	0.623194	9.229397	6.347838	0.000706	0.029061
147	Gadd45g	-0.626127	8.762779	-6.288403	0.000742	0.029398
148	Dlg2	0.613869	4.659152	6.163128	0.000826	0.031039
149	Ets2	-0.596070	9.482493	-6.134975	0.000846	0.031271
150	Cspg4	-0.735126	8.705591	-6.065576	0.000899	0.031931
151	Pdk4	1.203111	5.237122	5.978108	0.000970	0.033101
152	Prr13	0.627845	10.406215	5.976964	0.000971	0.033101
153	Psmf1	-0.599616	5.400454	-5.907930	0.001032	0.033778
154	Lrig1	-0.775384	10.316201	-5.906379	0.001034	0.033778
155	Dpp7	-0.602565	8.118704	-5.834983	0.001102	0.034718
156	Wars	0.649072	7.887403	5.811477	0.001125	0.034807
157	Dmpk	-0.932881	7.473077	-5.804037	0.001133	0.034807
158	Phactr1	-1.114158	8.270404	-5.796496	0.001141	0.034807
159	Plin4	-1.199042	7.715632	-5.792890	0.001144	0.034807
160	Lrrk2	0.591076	6.850937	5.789498	0.001148	0.034865
161	Ypel5	0.709533	9.060197	5.764418	0.001174	0.035057
162	Akr1b7	0.907198	5.466902	5.757785	0.001181	0.035057
163	Bmp2k	-0.778222	7.753361	-5.766863	0.001171	0.035057
164	Csn3	0.992612	7.339256	5.749166	0.001190	0.035236
165	Nrip2	0.871862	6.920145	5.729696	0.001212	0.035480
166	B4galt5	-0.643839	5.342762	-5.677440	0.001271	0.035881
167	Fastkd1	0.611068	7.330663	5.658485	0.001293	0.036090
168	Naip2	0.811971	7.150355	5.597499	0.001367	0.037133
169	Pparg	-0.962716	7.980085	-5.600352	0.001364	0.037133
170	Pdk1	-0.797515	7.883736	-5.551202	0.001427	0.038109
171	Sf3b1	-0.789371	6.459089	-5.462114	0.001551	0.039106
172	Nfix	-0.613159	8.682556	-5.450242	0.001569	0.039342
173	Ccng2	-0.776947	6.616898	-5.405501	0.001636	0.040026
174	Mga	-0.851886	6.279599	-5.336158	0.001748	0.041146
175	Srgn	0.699474	7.932847	5.233246	0.001930	0.043028
176	Mapk8ip1	-0.665751	6.477866	-5.229657	0.001936	0.043134
177	Abhd1	0.605183	6.460918	5.186021	0.002020	0.044067
178	Mrgprf	-0.652085	6.943122	-5.181912	0.002028	0.044113
179	Lipg	-0.884078	8.882551	-5.156814	0.002079	0.044669
180	Ifitm6	0.712596	4.700088	5.142685	0.002108	0.044950
181	Ifna2	-0.708373	5.622176	-5.109937	0.002176	0.045843
182	Noct	-1.049426	9.657526	-5.107516	0.002182	0.045864
183	Gadd45b	-1.134996	8.811065	-5.097570	0.002203	0.045966
184	Mef2a	-0.602866	9.136150	-5.094697	0.002209	0.046052

Appendix Table 2. The complete list of DEGs of Set1 (Continuous)

No.	symbol	logFC	AveExpr	t	P.Value	adj.P.Val
185	Plat	-1.199145	8.117924	-5.063212	0.002279	0.046781
186	LOC102642819	-0.658984	5.882889	-5.040220	0.002332	0.047133
187	Ppargc1a	-0.686334	4.082342	-4.984941	0.002464	0.048236
188	Nfkbia	-1.001156	10.288093	-4.979486	0.002477	0.048236
189	Ero1l	-0.681598	11.082389	-4.933393	0.002595	0.049339
190	Hspa2	0.610289	6.143104	4.912070	0.002651	0.049886
191	H2-Q4	-0.730963	9.562344	-4.904081	0.002673	0.050067
192	Ikbke	0.622125	6.485807	4.830996	0.002879	0.051656
193	Flt3l	0.693896	7.710814	4.819452	0.002913	0.051814
194	Sub1	-0.702792	6.177993	-4.797402	0.002979	0.052107
195	Tpcn2	-0.662557	7.649166	-4.789642	0.003003	0.052275
196	Pla2g4a	0.968514	10.546383	4.721519	0.003222	0.053925
197	Prkd2	0.632171	5.943234	4.721270	0.003223	0.053925
198	Lrrc51	0.852833	8.329948	4.656349	0.003448	0.055387
199	Fdft1	-0.639879	9.717128	-4.644893	0.003490	0.055607
200	Plau	-0.690808	8.670617	-4.602365	0.003649	0.057156
201	Eno2	-1.037632	5.915293	-4.601372	0.003653	0.057175
202	Trp53	0.613896	7.874134	4.580264	0.003735	0.057640
203	Lcn2	2.270332	7.216283	4.548270	0.003864	0.058605
204	AA408650	-1.073851	6.467952	-4.535724	0.003916	0.059004
205	Plekho1	-0.741771	8.527129	-4.525372	0.003959	0.059354
206	Per2	-0.743774	5.532967	-4.516216	0.003998	0.059750
207	Angptl4	-0.802406	10.469830	-4.504326	0.004049	0.060065
208	Fam134b	-0.684044	9.204207	-4.468062	0.004209	0.061476
209	Fhod3	-0.661618	4.490288	-4.437799	0.004348	0.062429
210	Mtss1	-0.795983	8.918592	-4.392976	0.004564	0.064353
211	Thbs1	-1.342196	6.571779	-4.366203	0.004698	0.065455
212	Dkk3	-0.821764	7.114756	-4.324064	0.004919	0.067009
213	Hipk2	-0.626969	7.025453	-4.295266	0.005077	0.068023
214	Slc39a6	-0.595588	8.379939	-4.249947	0.005337	0.069844
215	Hist1h1c	-0.595255	11.250690	-4.114987	0.006203	0.075371
216	Azin1	-0.940745	11.120883	-4.057904	0.006616	0.077371
217	Slc5a3	-0.820695	5.001783	-4.041325	0.006742	0.078051
218	Asap1	-0.604609	8.024729	-4.024907	0.006869	0.078526
219	Zfpm1	-0.607761	6.023392	-4.012683	0.006965	0.079033
220	Ttc28	-0.664244	7.068244	-3.936505	0.007600	0.082529
221	Pla2g2e	0.800782	8.569137	3.935241	0.007612	0.082607
222	Plxdc1	-1.061830	6.188863	-3.915306	0.007789	0.083268
223	Egln1	-0.623186	7.838358	-3.913733	0.007803	0.083289
224	Gprc5b	-0.881260	7.923260	-3.906713	0.007866	0.083489
225	Sdccag8	0.778632	5.964213	3.899684	0.007931	0.083801
226	Cpeb4	-1.079149	8.591538	-3.886364	0.008054	0.084526
227	Acsbg1	0.863988	6.655097	3.881284	0.008102	0.084843
228	Sox5	-0.619884	7.685893	-3.859929	0.008305	0.085800
229	Ms4a4d	0.850803	10.369904	3.856981	0.008334	0.085996
230	Olfml2b	-1.055820	9.446832	-3.848173	0.008420	0.086177

Appendix Table 2. The complete list of DEGs of Set1 (Continuous)

No.	symbol	logFC	AveExpr	t	P.Value	adj.P.Val
231	Wisp2	-0.916531	8.439451	-3.847757	0.008424	0.086177
232	Zfx	-0.679706	5.001863	-3.787341	0.009041	0.088861
233	F3	-0.788704	8.586142	-3.783026	0.009087	0.088942
234	Il11	0.973276	8.261174	3.772145	0.009204	0.089518
235	Runx1t1	-0.610587	8.881100	-3.746050	0.009491	0.090321
236	Ppargc1b	-0.675491	7.098651	-3.719428	0.009795	0.092114
237	Pdcd4	0.663663	7.876260	3.668055	0.010412	0.095117
238	Vcl	-0.629020	11.194121	-3.647688	0.010668	0.096067
239	Ddit4	-1.276578	10.012531	-3.622560	0.010994	0.097688
240	Svil	0.637322	7.931195	3.614845	0.011097	0.098161
241	Tlr2	-0.928995	9.891618	-3.584727	0.011506	0.099784

logFC, log2-fold-change
AveExpr, Average log2-expression for the probe over all arrays and channels
t, moderated t-statistic
P.Value, raw p-value
adj.P.Val, Benjamini and Hochberg FDR adjusted p-value

References

1. Zhang Q, Riddle RC, Clemens TL (2015) Bone and the regulation of global energy balance. J Intern Med 277:681–689

2. Findlay DM (2018) Biology of Bone and the Interaction of Bone with Other Organ Systems. In: Multiscale Mechanobiology of Bone Remodeling and Adaptation. Springer, pp 259–287

3. Sato M, Asada N, Kawano Y, et al (2013) Osteocytes regulate primary lymphoid organs and fat metabolism. Cell Metab 18:749–758

4. Movérare-Skrtic S, Henning P, Liu X, et al (2014) Osteoblast-derived WNT16 represses osteoclastogenesis and prevents cortical bone fragility fractures. Nat Med 20:1279–1288

5. Oldknow KJ, MacRae VE, Farquharson C (2015) Endocrine role of bone: Recent and emerging perspectives beyond osteocalcin. J Endocrinol 225:R1–R19

6. Karsenty G, Oury F (2012) Biology Without Walls: The Novel Endocrinology of Bone. Annu Rev Physiol 74:87–105

7. DiGirolamo DJ, Clemens TL, Kousteni S (2012) The skeleton as an endocrine organ. Nat Rev Rheumatol 8:674–683

8. Yoshikawa Y, Kode A, Xu L, et al (2011) Genetic evidence points to an osteocalcin-independent influence of osteoblasts on energy metabolism. J Bone Miner Res 26:2012–2025

9. Qing H, Ardeshirpour L, Divieti Pajevic P, et al (2012) Demonstration of osteocytic perilacunar/canalicular remodeling in mice during lactation. J Bone Miner Res 27:1018–1029

10. Capulli M, Paone R, Rucci N (2014) Osteoblast and osteocyte: Games without frontiers. Arch Biochem Biophys 561:3–12

11. Teti A, Zallone A (2009) Do osteocytes contribute to bone mineral homeostasis? Osteocytic osteolysis revisited. Bone 44:11–16

12. Lee S-H, Park S-J, Kim K-N, et al (2016) Coronary Calcification Is Reversely Related with Bone and Hair Calcium: The Relationship among Different Calcium Pools in Body. J Bone Metab 23:191

13. Xiong J, Piemontese M, Onal M, et al (2015) Osteocytes, not osteoblasts or lining cells, are the main source of the RANKL required for osteoclast formation in remodeling bone. PLoS One 10:1–19

14. Spiegel A, Kalinkovich A, Shivtiel S, et al (2008) Stem Cell Regulation via Dynamic Interactions of the Nervous and Immune Systems with the Microenvironment. Cell Stem Cell 3:484–492

15. Asada N, Katayama Y, Sato M, et al (2013) Matrix-embedded osteocytes regulate mobilization of hematopoietic stem/progenitor cells. Cell Stem Cell 12:737–747

16. Katayama Y, Battista M, Kao WM, et al (2006) Signals from the sympathetic nervous system regulate hematopoietic stem cell egress from bone marrow. Cell 124:407–421

17. Li S-D, Chen Y-B, Qiu L-G, Qin M-Q (2017) G-CSF Indirectly Induces Apoptosis of Osteoblasts During Hematopoietic Stem Cell Mobilization. Clin Transl Sci 1–5

18. Jung WC, Levesque JP, Ruitenberg MJ (2017) It takes nerve to fight back: The significance of neural innervation of the bone marrow and spleen for immune function. Semin Cell Dev Biol 61:60–70

19. Vignaux G, Besnard S, Ndong J, et al (2013) Bone remodeling is regulated by inner ear vestibular signals. J Bone Miner Res 28:2136–2144

20. Vignaux G, Ndong JDLC, Perrien DS, Elefteriou F (2015) Inner ear vestibular signals regulate bone remodeling via the sympathetic nervous system. J Bone Miner Res 30:1103–1111

21. Towler DA (2017) "Osteotropic" Wnt/LRP Signals. Arterioscler Thromb Vasc Biol 37:392–395

22. Ramasamy SK, Kusumbe AP, Itkin T, et al (2016) Regulation of Hematopoiesis and Osteogenesis by Blood Vessel-Derived Signals. Annu Rev Cell Dev Biol 32:649–675

23. Morrison SJ, Scadden DT (2014) The bone marrow niche for haematopoietic stem cells. Nature 505:327–334

24. Méndez-Ferrer S, Frenette PS (2007) Hematopoietic stem cell trafficking: Regulated adhesion and attraction to bone marrow microenvironment. Ann N Y Acad Sci 1116:392–413

25. Shwartz Y, Blitz E, Zelzer E (2013) One load to rule them all: Mechanical control of the musculoskeletal system in development and aging. Differentiation 86:104–111

26. Rolfe R, Roddy K, Murphy P (2013) Mechanical regulation of skeletal development. Curr Osteoporos Rep 11:107–116

27. Lebrasseur NK, Achenbach SJ, Melton LJ, et al (2012) Skeletal muscle mass is associated with bone geometry and microstructure and serum insulin-like growth factor binding protein-2 levels in adult women and men. J Bone Miner Res 27:2159–2169

28. Shen H, Grimston S, Civitelli R, Thomopoulos S (2015) Deletion of Connexin43 in Osteoblasts/Osteocytes Leads to Impaired Muscle Formation in Mice. J Bone Miner Res 30:596–605

29. Dankbar B, Fennen M, Brunert D, et al (2015) Myostatin is a direct regulator of osteoclast differentiation and its inhibition reduces inflammatory joint destruction in mice. Nat Med 21:1085–1090

30. Liu W, Zhou L, Zhou C, et al (2016) GDF11 decreases bone mass by stimulating osteoclastogenesis and inhibiting osteoblast differentiation. Nat Commun 7:12794

31. Wood CL, Pajevic PD, Gooi JH (2017) Osteocyte secreted factors inhibit skeletal muscle differentiation. Bone Reports 6:74–80

32. Ducy P, Amling M, Takeda S, et al (2000) Leptin inhibits bone formation through a hypothalamic relay: a central control of bone mass. Cell 100:197–207

33. Takeda S, Elefteriou F, Levasseur R, et al (2002) Leptin regulates bone formation via the sympathetic nervous system. Cell 111:305–317

34. Hinoi E, Gao N, Jung DY, et al (2008) The sympathetic tone mediates leptin's inhibition of insulin secretion by modulating osteocalcin bioactivity. J Cell Biol 183:1235–1242

35. Lee NK, Sowa H, Hinoi E, et al (2007) Endocrine Regulation of Energy Metabolism by the Skeleton. Cell 130:456–469

36. Wei J, Hanna T, Suda N, et al (2014) Osteocalcin promotes β-cell proliferation during development and adulthood through Gprc6a. Diabetes 63:1021–1031

37. Sapir-Koren R, Livshits G (2014) Osteocyte control of bone remodeling: is sclerostin a key molecular coordinator of the balanced bone resorption–formation cycles? Osteoporos Int 25:2685–2700

38. Baron R, Kneissel M (2013) WNT signaling in bone homeostasis and disease: from human mutations to treatments. Nat Med 19:179–192

39. Kang S, Bajnok L, Longo KA, et al (2005) Effects of Wnt Signaling on Brown Adipocyte Differentiation and Metabolism Mediated by PGC-1 . Mol Cell Biol 25:1272–1282

40. Kang S, Bennett CN, Gerin I, et al (2007) Wnt signaling stimulates osteoblastogenesis of mesenchymal precursors by suppressing CCAAT/enhancer-binding protein α and peroxisome proliferator-activated receptor γ. J Biol Chem 282:14515–14524

41. Ukita M, Yamaguchi T, Ohata N, Tamura M (2016) Sclerostin Enhances Adipocyte Differentiation in 3T3-L1 Cells. J Cell Biochem 117:1419–1428

42. Fulzele K, Lai F, Dedic C, et al (2017) Osteocyte-Secreted Wnt Signaling Inhibitor Sclerostin Contributes to Beige Adipogenesis in Peripheral Fat Depots. J Bone Miner Res 32:373–384

43. Ma YHV, Schwartz A V., Sigurdsson S, et al (2014) Circulating sclerostin associated with vertebral bone marrow fat in older men but not women. J Clin Endocrinol Metab 99:E2584–E2590

44. Sheng Z, Tong D, Ou Y, et al (2012) Serum sclerostin levels were positively correlated with fat mass and bone mineral density in Central South Chinese postmenopausal women. Clin Endocrinol (Oxf) 76:797–801

45. Amrein K, Amrein S, Drexler C, et al (2012) Sclerostin and its association with physical activity, age, gender, body composition, and bone mineral content in healthy adults. J Clin Endocrinol Metab 97:148–54

46. Hirai T (2017) Circadian clock and bone biology. J Oral Biosci 59:179–183

47. te Boekhorst V, Preziosi L, Friedl P (2016) Plasticity of cell migration in vivo and in silico. Annu Rev Cell Dev Biol 32:491–526

48. Moustafa A, Sugiyama T, Prasad J, et al (2012) Mechanical loading-related changes in osteocyte sclerostin expression in mice are more closely associated with the subsequent osteogenic response than the peak strains engendered. Osteoporos Int 23:1225–1234

49. Galea GL, Lanyon LE, Price JS (2017) Sclerostin's role in bone's adaptive response to mechanical loading. Bone 96:38–44

50. You L, Temiyasathit S, Lee P, et al (2008) Osteocytes as mechanosensors in the inhibition of

bone resorption due to mechanical loading. Bone 42:172–179

51. Wijenayaka AR, Kogawa M, Lim HP, et al (2011) Sclerostin stimulates osteocyte support of osteoclast activity by a RANKL-dependent pathway. PLoS One 6:

52. Atkins GJ, Rowe PS, Lim HP, et al (2011) Sclerostin is a locally acting regulator of late-osteoblast/preosteocyte differentiation and regulates mineralization through a MEPE-ASARM-dependent mechanism. J Bone Miner Res 26:1425–1436

53. Kogawa M, Wijenayaka AR, Ormsby RT, et al (2013) Sclerostin regulates release of bone mineral by osteocytes by induction of carbonic anhydrase 2. J Bone Miner Res 28:2436–2448

54. Lefrançais E, Ortiz-Muñoz G, Caudrillier A, et al (2017) The lung is a site of platelet biogenesis and a reservoir for haematopoietic progenitors. Nature 544:105–109

55. Robin M, Almeida C, Azaïs T, et al (2016) Involvement of 3D osteoblast migration and bone apatite during in vitro early osteocytogenesis. Bone 88:146–156

56. Kim K-J, Choi S, Sang Cho Y, et al (2017) Magnesium ions enhance infiltration of osteoblasts in scaffolds via increasing cell motility. J Mater Sci Mater Med 28:96

57. Mooren FC (2015) Magnesium and disturbances in carbohydrate metabolism. Diabetes, Obes Metab 17:813–823

58. Plotkin LI, Bellido T (2016) Osteocytic signalling pathways as therapeutic targets for bone fragility. Nat Rev Endocrinol 12:593–605

59. Adachi T, Aonuma Y, Ito S ichi, et al (2009) Osteocyte calcium signaling response to bone matrix deformation. J Biomech 42:2507–2512

60. Adachi T, Aonuma Y, Tanaka M, et al (2009) Calcium response in single osteocytes to locally applied mechanical stimulus: Differences in cell process and cell body. J Biomech 42:1989–1995

61. Ishihara Y, Sugawara Y, Kamioka H, et al (2014) Oscillatory intracellular Ca2+ responses in living bone. J Oral Biosci 56:49–53

62. McClung MR, Grauer A, Boonen S, et al (2014) Romosozumab in Postmenopausal Women with Low Bone Mineral Density. N Engl J Med 370:412–420

63. Sethi J, Vidal-Puig A (2010) Wnt signalling and the control of cellular metabolism. Biochem J 427:1–17

64. Karner CM, Long F (2017) Wnt signaling and cellular metabolism in osteoblasts. Cell Mol Life Sci 74:1649–1657

65. Wang Z, Odagaki N, Tanaka T, et al (2016) Alternation in the gap-junctional intercellular communication capacity during the maturation of osteocytes in the embryonic chick calvaria. Bone 91:20–29

66. Sugawara Y, Kamioka H, Ishihara Y, et al (2013) The early mouse 3D osteocyte network in the presence and absence of mechanical loading. Bone 52:189–196

67. Weinbaum S, Cowin SC, Zeng Y (1994) A model for the excitation of osteocytes by mechanical loading-induced bone fluid shear stresses. J Biomech 27:339–360

68. Kamioka H, Honjo T, Takano-Yamamoto T (2001) A three-dimensional distribution of osteocyte processes revealed by the combination of confocal laser scanning microscopy and differential interference contrast microscopy. Bone 28:145–149

69. Jing D, Baik AD, Lu XL, et al (2014) In situ intracellular calcium oscillations in osteocytes in intact mouse long bones under dynamic mechanical loading. FASEB J 28:1582–1592

70. Phipson B, Lee S, Majewski IJ, et al (2016) Robust hyperparameter estimation protects against hypervariable genes and improves power to detect differential expression. Ann Appl Stat 10:946–963

71. Ashburner M, Ball CA, Blake JA, et al (2000) Gene Ontology: tool for the unification of biology. Nat Genet 25:25–29

72. Carbon S, Dietze H, Lewis SE, et al (2017) Expansion of the Gene Ontology knowledgebase and resources. Nucleic Acids Res 45:D331–D338

73. Ogata H, Goto S, Sato K, et al (1999) KEGG: Kyoto Encyclopedia of Genes and Genomes. Nucleic Acids Res 27:29–34

74. Huang D, Sherman BT, Tan Q, et al (2007) The DAVID Gene Functional Classification Tool: a novel biological module-centric algorithm to functionally analyze large gene lists. Genome Biol 8:R183

75. Mering C v. (2003) STRING: a database of predicted functional associations between proteins. Nucleic Acids Res 31:258–261

76. Kohl M, Wiese S, Warscheid B (2011) Cytoscape: Software for Visualization and Analysis of Biological Networks. In: Hamacher M, Eisenacher M, Stephan C (eds) Data mining in proteomics: from standards to applications, 1st ed. Springer, pp 291–303

77. Yip KY, Yu H, Kim PM, et al (2006) The tYNA platform for comparative interactomics: a web tool for managing, comparing and mining multiple networks. Bioinformatics 22:2968–2970

78. Kamioka H, Sugawara Y, Murshid SA, et al (2006) Fluid Shear Stress Induces Less Calcium Response in a Single Primary Osteocyte Than in a Single Osteoblast: Implication of Different Focal Adhesion Formation. J Bone Miner Res 21:1012–1021

79. Frangos J, Eskin S, McIntire L, Ives C (1985) Flow effects on prostacyclin production by cultured human endothelial cells. Science (80-) 227:1477–1479

80. Odagaki N, Ishihara Y, Wang Z, et al (2018) Role of Osteocyte-PDL Crosstalk in Tooth Movement via SOST/Sclerostin. J Dent Res 97:1374–1382

81. Yu K, Sellman DP, Bahraini A, et al (2017) Mechanical loading disrupts osteocyte plasma membranes which initiates mechanosensation events in bone. J Orthop Res 1–10

82. Wu C, Rankin EB, Castellini L, et al (2015) Oxygen-sensing PHDs regulate bone homeostasis through the modulation of osteoprotegerin. Genes Dev 29:817–831

83. Shen X, Wan C, Ramaswamy G, et al (2009) Prolyl hydroxylase inhibitors increase neoangiogenesis and callus formation following femur fracture in mice. J Orthop Res 27:1298–1305

84. HUANG J, LIU L, FENG M, et al (2015) Effect of CoCl2 on fracture repair in a rat model of bone fracture. Mol Med Rep 12:5951–5956

85. Stewart R, Goldstein J, Eberhardt A, et al (2011) Increasing Vascularity to Improve Healing of a Segmental Defect of the Rat Femur. J Orthop Trauma 25:472–476

86. Zhang W, Li G, Deng L, et al (2012) New bone formation in a true bone ceramic scaffold loaded with desferrioxamine in the treatment of segmental bone defect: a preliminary study. J Orthop Sci 17:289–298

87. Wan C, Gilbert SR, Wang Y, et al (2008) Activation of the hypoxia-inducible factor-1 pathway accelerates bone regeneration. Proc Natl Acad Sci 105:686–691

88. Liu X, Tu Y, Zhang L, et al (2014) Prolyl Hydroxylase Inhibitors Protect from the Bone Loss in Ovariectomy Rats by Increasing Bone Vascularity. Cell Biochem Biophys 69:141–149

89. Peng J, Lai ZG, Fang ZL, et al (2014) Dimethyloxalylglycine Prevents Bone Loss in Ovariectomized C57BL/6J Mice through Enhanced Angiogenesis and Osteogenesis. PLoS One 9:e112744

90. Bentovim L, Amarilio R, Zelzer E (2013) HIF1 is a central regulator of collagen hydroxylation and secretion under hypoxia during bone development. Development 140:248–248

91. Kim J, Tchernyshyov I, Semenza GL, Dang C V. (2006) HIF-1-mediated expression of pyruvate dehydrogenase kinase: A metabolic switch required for cellular adaptation to hypoxia. Cell Metab 3:177–185

92. Wenger RH, Stiehl DP, Camenisch G (2005) Integration of Oxygen Signaling at the Consensus HRE. Sci Signal 2005:re12–re12

93. Fujiwara M, Kubota T, Wang W, et al (2016) Successful induction of sclerostin in human-derived fibroblasts by 4 transcription factors and its regulation by parathyroid hormone, hypoxia, and prostaglandin E2. Bone 85:91–98

94. Lin C, Jiang X, Dai Z, et al (2009) Sclerostin Mediates Bone Response to Mechanical Unloading Through Antagonizing Wnt/β-Catenin Signaling. J Bone Miner Res 24:1651–1661

95. Winkler DG (2003) Osteocyte control of bone formation via sclerostin, a novel BMP antagonist. EMBO J 22:6267–6276

96. Ellies DL, Viviano B, McCarthy J, et al (2006) Bone Density Ligand, Sclerostin, Directly Interacts With LRP5 but Not LRP5G171V to Modulate Wnt Activity. J Bone Miner Res 21:1738–1749

97. McGee-Lawrence ME, Ryan ZC, Carpio LR, et al (2013) Sclerostin deficient mice rapidly heal bone defects by activating β-catenin and increasing intramembranous ossification. Biochem Biophys Res Commun 441:886–890

98. Cosman F, Crittenden DB, Adachi JD, et al (2016) Romosozumab Treatment in Postmenopausal Women with Osteoporosis. N Engl J Med 375:1532–1543

99. Saag KG, Petersen J, Brandi ML, et al (2017) Romosozumab or Alendronate for Fracture Prevention in Women with Osteoporosis. N Engl J Med 377:1417–1427

100. Chen NX, Ryder KD, Pavalko FM, et al (2000) Ca(2+) regulates fluid shear-induced cytoskeletal reorganization and gene expression in osteoblasts. Am J Physiol Physiol 278:C989-97

101. Dai Z, Chung SK, Miao D, et al (2011) Sodium/myo-inositol cotransporter 1 and myo-inositol are essential for osteogenesis and bone formation. J Bone Miner Res 26:582–590

102. Vande Velde C, Cizeau J, Dubik D, et al (2000) BNIP3 and Genetic Control of Necrosis-Like Cell Death through the Mitochondrial Permeability Transition Pore. Mol Cell Biol 20:5454–5468

103. Liu J, Yuan C, Pu L, Wang J (2017) Nutrient deprivation induces apoptosis of nucleus pulposus cells via activation of the BNIP3/AIF signalling pathway. Mol Med Rep 16:7253–7260

104. Liu J, Wang J, Zhou Y (2012) Upregulation of BNIP3 and translocation to mitochondria in nutrition deprivation induced apoptosis in nucleus pulposus cells. Jt Bone Spine 79:186–191

105. Prideaux M, Dallas SL, Zhao N, et al (2015) Parathyroid hormone induces bone cell motility and loss of mature osteocyte phenotype through L-calcium channel dependent and independent mechanisms. PLoS One 10:1–25

106. Ullah M, Stich S, Notter M, et al (2013) Transdifferentiation of mesenchymal stem cells-derived adipogenic-differentiated cells into osteogenic- or chondrogenic-differentiated cells proceeds via dedifferentiation and have a correlation with cell cycle arresting and driving genes. Differentiation 85:78–90

107. Bellido T, Ali AA, Gubrij I, et al (2005) Chronic Elevation of Parathyroid Hormone in Mice Reduces Expression of Sclerostin by Osteocytes: A Novel Mechanism for Hormonal Control of Osteoblastogenesis. Endocrinology 146:4577–4583

108. Ameri K, Rajah AM, Nguyen V, et al (2013) Nuclear Localization of the Mitochondrial Factor HIGD1A during Metabolic Stress. PLoS One 8:

109. An HJ, Shin H, Jo SG, et al (2011) The survival effect of mitochondrial Higd-1a is associated with suppression of cytochrome C release and prevention of caspase activation. Biochim Biophys Acta - Mol Cell Res 1813:2088–2098

110. Yokomoto-Umakoshi M, Kanazawa I, Takeno A, et al (2016) Activation of AMP-activated protein kinase decreases receptor activator of NF-κB ligand expression and increases sclerostin expression by inhibiting the mevalonate pathway in osteocytic MLO-Y4 cells. Biochem Biophys Res Commun 469:791–796

111. Tascau L, Gardner T, Anan H, et al (2016) Activation of Protein Kinase A in Mature Osteoblasts Promotes a Major Bone Anabolic Response. Endocrinology 157:112–126

112. Takeno A, Kanazawa I, Tanaka K, et al (2015) Activation of AMP-activated protein kinase protects against homocysteine-induced apoptosis of osteocytic MLO-Y4 cells by regulating the expressions of NADPH oxidase 1 (Nox1) and Nox2. Bone 77:135–141

113. Zhan P, Zhao S, Yan H, et al (2017) α-enolase promotes tumorigenesis and metastasis via regulating AMPK/mTOR pathway in colorectal cancer. Mol Carcinog 56:1427–1437

114. de Araujo RMS, Oba Y, Moriyama K (2007) Identification of genes related to mechanical stress in human periodontal ligament cells using microarray analysis. J Periodontal Res 42:15–22

115. Hamamura K, Liu Y, Yokota H (2008) Microarray analysis of thapsigargin - Induced stress to the endoplasmic reticulum of mouse osteoblasts. J Bone Miner Metab 26:231–240

116. Kim H-S, Choi D-Y, Yun SJ, et al (2012) Proteomic Analysis of Microvesicles Derived from Human Mesenchymal Stem Cells. J Proteome Res 11:839–849

117. Li J, Ahmad T, Spetea M, et al (2001) Bone Reinnervation After Fracture: A Study in the Rat. J Bone Miner Res 16:1505–1510

118. Strange-Vognsen HH, Laursen H (1997) Nerves in Human Epiphyseal Uncalcified Cartilage. J Pediatr Orthop B 6:56–58

119. Hukkanen M, Konttinen YT, Santavirta S, et al (1993) Rapid proliferation of calcitonin gene-related peptide-immunoreactive nerves during healing of rat tibial fracture suggests neural involvement in bone growth and remodelling. Neuroscience 54:969–979

120. Liu M, Sun Y, Zhang Q (2018) Emerging Role of Extracellular Vesicles in Bone Remodeling. J Dent Res. https://doi.org/10.1177/0022034518764411

121. Qin Y, Peng Y, Zhao W, et al (2017) Myostatin inhibits osteoblastic differentiation by suppressing osteocyte-derived exosomal microRNA-218: A novel mechanism in muscle-bone communication. J Biol Chem 292:11021–11033

122. Herrera MB, Fonsato V, Gatti S, et al (2010) Human liver stem cell-derived microvesicles accelerate hepatic regeneration in hepatectomized rats. J Cell Mol Med 14:1605–1618

123. Lai RC, Arslan F, Lee MM, et al (2010) Exosome secreted by MSC reduces myocardial ischemia/reperfusion injury. Stem Cell Res 4:214–222

124. Bruno S, Grange C, Deregibus MC, et al (2009) Mesenchymal Stem Cell-Derived Microvesicles Protect Against Acute Tubular Injury. J Am Soc Nephrol 20:1053–1067

125. Aguirre JI, Plotkin LI, Stewart SA, et al (2006) Osteocyte apoptosis is induced by weightlessness in mice and precedes osteoclast recruitment and bone loss. J Bone Miner Res 21:605–615

126. Manolagas SC, Parfitt AM (2010) What old means to bone. Trends Endocrinol Metab 21:369–374

127. Takano-Yamamoto T (2014) Osteocyte function under compressive mechanical force. Jpn Dent Sci Rev 50:29–39

128. Plotkin LI (2014) Apoptotic osteocytes and the control of targeted bone resorption. Curr Osteoporos Rep 12:121–126

129. Goda N, Kanai M (2012) Hypoxia-inducible factors and their roles in energy metabolism. Int J Hematol 95:457–463

130. Stegen S, Stockmans I, Moermans K, et al (2018) Osteocytic oxygen sensing controls bone mass through epigenetic regulation of sclerostin. Nat Commun 9:

131. Ahmad Waza A, Ahmad Bhat S, Ul Hussain M, Ganai BA (2018) Connexin 43 and ATP-sensitive potassium channels crosstalk: a missing link in hypoxia/ischemia stress. Cell Tissue Res 371:213–222

132. Matsushita S, Kurihara H, Watanabe M, et al (2006) Alterations of Phosphorylation State of Connexin 43 during Hypoxia and Reoxygenation Are Associated with Cardiac Function. J Histochem Cytochem 54:343–353

133. Matsushita S, Kurihara H, Watanabe M, et al (2011) Inhibition of connexin43 dephosphorylation is involved in protective effects of diltiazem on cardiac function during hypoxic injury. Histol Histopathol 26:315–22

134. ZEEVILEVIN N, BARAC Y, REISNER Y, et al (2005) Gap junctional remodeling by hypoxia in cultured neonatal rat ventricular myocytes. Cardiovasc Res 66:64–73

135. Cowan DB, Jones M, Garcia LM, et al (2003) Hypoxia and Stretch Regulate Intercellular Communication in Vascular Smooth Muscle Cells Through Reactive Oxygen Species Formation. Arterioscler Thromb Vasc Biol 23:1754–1760

136. Chen J, He L, Dinger B, et al (2002) Chronic hypoxia upregulates connexin43 expression in rat carotid body and petrosal ganglion. J Appl Physiol 92:1480–1486

137. Weng T, Xie Y, Huang J, et al (2014) Inactivation of Vhl in Osteochondral Progenitor Cells Causes High Bone Mass Phenotype and Protects Against Age-Related Bone Loss in Adult Mice. J Bone Miner Res 29:820–829

138. Loots GG, Robling AG, Chang JC, et al (2018) Vhl deficiency in osteocytes produces high bone mass and hematopoietic defects. Bone 116:307–314

139. Yellowley CE, Genetos DC (2019) Hypoxia Signaling in the Skeleton: Implications for Bone Health. Curr Osteoporos Rep 17:26–35

140. Bromage TG, Lacruz RS, Hogg R, et al (2009) Lamellar bone is an incremental tissue reconciling enamel rhythms, body size, and organismal life history. Calcif Tissue Int 84:388–404

141. Bromage TG, Hogg RT, Lacruz RS, Hou C (2012) Primate enamel evinces long period biological timing and regulation of life history. J Theor Biol 305:131–144

142. Bromage TG, Janal MN (2014) The Havers-Halberg oscillation regulates primate tissue and organ masses across the life-history continuum. Biol J Linn Soc 112:649–656

143. Yuan G, Hua B, Yang Y, et al (2017) The Circadian Gene Clock Regulates Bone Formation Via PDIA3. J Bone Miner Res 32:861–871

144. Maury E, Hong HK, Bass J (2014) Circadian disruption in the pathogenesis of metabolic syndrome. Diabetes Metab 40:338–346

145. Lloyd SA, Loiselle AE, Zhang Y, Donahue HJ (2014) Shifting paradigms on the role of connexin43 in the skeletal response to mechanical load. J Bone Miner Res 29:275–286